Mon. Not. R. Astron. Soc. **000**, 1–15 (2004) Printed 2 February 2008 (MN LaTeX style file v2.2)

arXiv:astro-ph/0412558v1 21 Dec 2004

Hot, Dense Matter Accretion onto a Black Hole

M. Yokosawa,[1]* S. Uematsu[1] and J. Abe[1]
[1]*Department of Astrophysics, Faculty of Natural Science, Ibaraki University, Mito Bunkyo 2-1-1 Post Num. 310-8512, Japan*

2 February 2008

ABSTRACT
The accretion of hot, dense matter which consists of heavy nuclei, free nucleons, degenerated electrons, photons and neutrinos is studied. The composition of free nucleons and their chemical potentials are provided through the equation of state for hot, dense matter proposed by Lattimer & Swesty (1991). The numbers of leptons are calculated through the reactions of neutrinos and through the simplified transfers of neutrinos in the accreting matter. The thermally equilibrium fluid structure of the accretion is solved. The angular momentum transfer in the disk is analyzed with the shear stress which is driven in the frame of the general relativity. When the mass of a central black hole and the accretion rate are selected as $M_{BH} \approx 3\mathrm{M}_{\odot}$ and $\dot{M} \approx 0.1\mathrm{M}_{\odot}\mathrm{sec}^{-1}$, which provide the typical luminosity of gamma ray bursts(GRBs), the fraction of free protons in the accreting matter becomes very small, $Y_p \approx 10^{-4}$, while that of free neutrons is closer to unity, $Y_n \approx 0.7$. Then the antielectron neutrinos $\bar{\nu}_e$ can freely escape through the disk but the electron neutrinos ν_e are almost absorbed in the disk. Thus the frequent collisions of $\bar{\nu}_e$ with ν_e over the disk couldn't be occurred. The accretion disk is cooled mainly by $\bar{\nu}_e$, which suppresses the increase of temperature and increases the density in the accreting matter such as $T \approx 3 \times 10^{10}$K and $\rho \approx 3 \times 10^{13}$g/cm^3 at the inner side of the disk. The scattering optical depths of $\bar{\nu}_e$ and ν_e then reach to be very large, $\tau_s(\bar{\nu}_e) \approx \tau_s(\nu_e) \approx 10^2$. Thus the accretion disk could be thermally unstable within the duration of diffusion time of neutrinos, $t_{diff} \approx 10$(ms). The ram pressure produced by many scattering of $\bar{\nu}_e$ are very strong, which might produce the neutrino driven wind or jets. The luminosity and mean energy of neutrinos, L_ν, $\bar{E}_\nu$, ejected from the disk increases with the specific angular momentum of a black hole. The mean energy is inversely proportional to the central mass, $\bar{E}_\nu \propto M_{BH}^{-1}$, while the luminosity L_ν is independent of its mass, M_{BH}. The diagram determining the physical properties of a central black hole from the observation of each flavor of neutrino is proposed.

Key words: accretion, accretion disks — black hole physics — gamma rays: bursts — neutrinos.

1 INTRODUCTION

An intense gamma-ray burst, GRB030329, allowed us to carry out the very detailed observations of optical, x-ray, and radio counterparts to the burst. Its photometry and spectroscopy led to the separation between the afterglow and SN contributions (Matheson et al. 2003; Kawabata et al. 2003; Lipkin et al. 2004). The SN component is similar to SN 1998bw; an unusual Type Ic SN (Stathakis et al. 2000; Ferdinado et al. 2001). It makes clear that at least some GRBs arise from core-collapse SNe. GRB030329 was seen as a double-pulsed burst with the total duration time of ∼30 sec (Vanderspek et al. 2004). Its total isotropic energy is $E_\gamma \sim 10^{52}$ erg. The GRBs with known redshifts distribute the emission energy E_γ over the wide range of energy such as 10^{48} erg $\geqslant E_\gamma \geqslant 10^{54}$erg(Greiner 2004). The duration times of GRBs extend from ∼10ms to $\sim 10^2$ sec(Piran 1999; Stern et al. 2001; Lloyd-Ronning & Ramirez-Ruiz 2002). The light curves of GRBs show really various profiles. However, to fully understand the emission mechanisms of the observed γ-ray bursts and of the afterglows one must have a firm handle on the generation process of the γ-ray bust.

The fireball model of the γ-ray bust has succeeded in understanding the characteristics of some light profiles of GRBs (Piran 1999). Its model was proposed to solve the compactness problem, that is, to understand both the short time variation of γ-ray radiation and the optically thin process in the emitting region of the γ-ray photons (Guibert, Fabian, & Rees 1983; Carigan, & Katz 1992). The solution of the fireball model requires the beaming jets with the emitting region relativistically moving to our direction. The two processes are proposed for the formation of the jets, one is the magnetohydrodynamical process (Thompson, Chang, & Quataert 2004; Lyutikov & Blandford 2003), and the other is the neutrino process (Popham, Woosley & Fryer 1999; Narayan, Piran, & Kumar 2001;

---

* E-mail: yokosawa@mx.ibaraki.ac.jp (MY)

Kohri, & Mineshige 2002; Di Matteo, Perna, & Narayan 2002). Further more the two different roles are expected for the neutrinos to form the jets. The frequent collisions between neutrinos and antineutrinos produce the fireball with light elements which expands relativistically in a funnel around a rotation axis. The other role is the acceleration of plasmas by the collisions of neutrinos with nucleons or electrons, which produces the neutrino driven jets. The sufficient collisions between ν and $\bar{\nu}$ at the central region of the accretion disk were proposed by Popham, Woosley & Fryer (1999). They assumed the accretion disk is optically thin for the transfer of neutrinos. But, Di Matteo, Perna, & Narayan (2002) showed that the accretion disk becomes optically thick for neutrino transfer and then the neutrinos trapped in the matter fall into a black hole.

However, the composition of accreting matter should be carefully considered. The production rates of neutrinos and their opacities directly depend on the density of free nucleons. Kohri, & Mineshige (2002) were thought in question whether the neutrinos can cool the accretion disk. They treated the accreting material in β equilibrium and showed that there exist just a small number of free nucleons and then the neutrino processes are no longer effective in cooling of the disk. This result is in a striking contrast to the previous works on the accretion disk in which the material almost consists of free nucleons produced by the photodisintegration process and the dominant cooling was carried out by neutrinos. Material at high temperature $T \geqslant 5 \times 10^9$K becomes in nuclear statistical equilibrium. Its composition of material depends on the number ratio of photon to baryon, $\psi = n_\gamma/\mu_H n_B$, where μ_H is the mean molecular weight, n_γ and n_B are the number densities of photons and baryons (Meyer et al. 1992). If ψ is large, $\psi \gg 1$, the baryons form a dissociated gas of nucleons and alpha particles. However, if ψ is of order unity or less, iron-group nuclei are typically favored. The ratio ψ is expressed as $\psi = 0.034 T_{11}^3/\rho_{12}$ in terms of the temperature T_{11} in units of 10^{11}K and the density ρ_{12} in units of 10^{12}g/cm^3. In the case of a typical accretion with $\dot{M} = 0.1$M$_\odot$/sec and $M_{BH} = 3$M$_\odot$, the temperature and the density become are $10^{10} < T < 10^{11}$(K) and $10^{11} < \rho < 10^{13}$(g/cm^3) at the inner region of the accretion disk. Then the values of ψ become as $\psi = 3.4 \times 10^{-2 \sim -3}$. One should treat the accreting matter with a large abundance of heavy nuclei. We determine the densities of free neutron and proton, alpha particle, and heavy nuclei by using the equation of state for hot, dense matter given by Lattimer & Swesty (1991). The changes of lepton number per a baryon, $\dot{Y}_l$, are calculated through the reactions of neutrinos with these baryons.

The thermal equilibrium structure of the accretion disk should be determined in the frame of a general relativity. MacFadyen & Woosley (1999) showed that the core-collapse in the evolved star with the main sequence mass , $M \geqslant 35$M$_\odot$, forms a black hole at the center with the rotating disk balanced with gravity when the evolved star has the some large specific angular momentum. Then the specific angular momentum parameter a of the falling matter into a black hole becomes larger to be $a \geqslant 0.9$. The falling velocity of the rotating disk is required to be very small in comparison with light velocity, since the time duration of some GRBs is a few seconds, i.e., $v_{fall} \approx scaleofdisk/durationtime \approx 10^2 r_g/afewsec \approx 10^{-3}c$, where r_g is the gravitational radius of a black hole and c is the light velocity. The accretion disk with slow falling velocity should be investigated in the frame of rotating spacetime. The heating rate due to viscosity is proportional to the shear stress $\sigma_{r\varphi}$. In the static spacetime its stress increases with the differential rotation of the accreting flow $\sigma_{r\varphi} \propto \partial_r \Omega$, where Ω is the angular velocity of the falling flow. In the rotating spacetime the differential rotation of the fluid observed in the frame co-rotating with spacetime is physically meaningful (Thorne, Price, & Macdonald 1986). In the extreme Kerr the relative angular velocity $\Omega - \omega$ has the maximum at the radius $r \approx 2r_g$ when Ω is the angular velocity of the Keplerian orbit and ω is the angular velocity of spacetime. It is convenient for the analysis of energy balance and of the transfer of angular momentum to introduce the orbiting frame with orthogonal tetrad which rotates with Keplarian velocity. In this paper the shear stress $\sigma_{r\varphi}$ and the transfer of angular momentum are solved by using the orbiting frame.

The power by advection contributes seriously to the energy balance in the accretion disk. The previous works on the accretion disk with neutrino loss had been studied in the frame of an advection-dominated accretion flow (Di Matteo, Perna, & Narayan 2002; Kohri, & Mineshige 2002; Narayan, Piran, & Kumar 2001; Popham, Woosley & Fryer 1999). The role of the advection in the energy balance depends on the velocity profile since the power by the advection is expressed as $P\vec{\nabla}\cdot\vec{v}$, where P and $\vec{v}$ are the pressure and velocity of the flow. When $\vec{\nabla} \cdot \vec{v} > 0$, the accreting matter is cooled by the expansion of fluid. On the other hand when $\vec{\nabla}\cdot\vec{v} < 0$, it is heated by the compression like as in the core-collapse in a supernova explosion. The radial velocity profile of the accreting flow is determined by the energy balance of the disk and by the transfer of angular momentum. The scale height at the inner portion of the disk with the temperature $T = 10^{10 \sim 11}$K is very thin. The angular velocity of the accretion disk is then approximated to be Keplerian. We determine the radial profile of the velocity by solving the transfer of angular momentum with the thermal energy balance of the disk and evaluate the efficiency of advection in the energy balance.

The thermal stability of the accretion disk might depend on the scattering optical depth of $\bar{\nu}_e$. The thermal energy in the disk is carried out mainly by $\bar{\nu}_e$. The collision frequency of $\bar{\nu}_e$ with the nucleons or electrons reaches to $N \approx \tau_{\bar{\nu}_e s}^2 \approx 10^4$ within the disk for the typical case of the accretion. The escaping time from the disk is then $t_{esc} \approx \tau_{\bar{\nu}_e s} H/c \approx 10$(ms), where H is the height of the disk. The thermal energy produced by viscous heating stays within the disk in the time $\Delta t \approx t_{esc}$ and might induce the thermal instability. We shall briefly analyze the thermal instability.

If the luminosity of each flavor of neutrino and its mean energy are observed the physics of GRBs will be cleared. We shall calculate the luminosity L_{ν_i} and the mean energy $\bar{E}_{\nu_i}$ for each type of neutrino ν_i emitted from the accretion disk. The diagram determining the mass of a central black hole, M_{BH}, and its specific angular momentum, a, from the observations of neutrinos is presented.

In this paper we study the accretion of hot dense matter onto a black hole. In Sect. 2 we describe the equation of state for the accreting hot, dense matter. The reactions of neutrinos and the changes of neutrino fractions are presented in section 2.2. The relativistic model of accretion disk with neutrino loss is given in Sect. 3. In Sect. 4 the results of thermally equilibrium disk are given. The profiles of compositions along the accretion flow are shown in section 4.1. The flow structure and chemical potentials of nucleons are depicted in section 4.2. The emissivities and opacities of neutrinos are presented in section 4.3. The luminosity and mean energy of neutrinos versus mass and angular momentum of a black hole are discussed in section 4.4. In Sect. 5 the thermal stability of the accretion disk is investigate. The neutrino transfer in homogeneous disk, changing rates of positrons and the dynamical properties of accretion disk are presented in Appendix. The cross sections of neutrinos, opacities, emission rates and the reaction rates of neutrinos are summarized in Tables, which are shown in Appendix.

2 ACCRETING DENSE MATTER AND REACTION OF NEUTRINOS

2.1 Equation of State for Accreting Dense Matter

It is important for the study of thermal and dynamical properties of massive accretion disks precisely to determine the fraction of free nucleons in the accreting matter. Its fraction provides the emissivities and absorptions of neutrinos. The mass fraction of free nucleons depends on the photon-to-baryon ratio ϕ(Burbidge et al. 1957; Meyer et al. 1992),

$$\phi = \frac{n_\gamma}{\rho N_A}, \tag{1}$$

where N_A is Avogadro's number. We compute ϕ in terms of the temperature T and density ρ as

$$\phi = \frac{1}{\pi^2}\frac{g_\gamma}{(hc/2\pi)^3}\frac{\zeta(3)(kT)^3}{\rho N_A} = 0.034\frac{T_{11}^3}{\rho_{12}}, \tag{2}$$

where g_γ is the helicity for photons. We evaluate the ratio ϕ for the neutrino dominated accreting flow (NDAF) given by Di Matteo, Perna, & Narayan (2002). The loci of NDAF with $\dot{M} = 0.1\mathrm{M}_\odot\mathrm{sec}^{-1}$ and the contours of $\phi(\rho, T)$ in the ρ — T plane are shown in Fig 1. The ratio ϕ on the flow is $\phi \leqslant 0.1$, showing little number density of photons. On the other hand the previous works on NDAF without Kohri, & Mineshige (2002) adopted the approximate formula for the mass fraction of free nucleons, X_{nuc}, (Qian & Woosley 1996) :

$$X_{nuc} = \frac{{T_{11}}^{9/8}}{\rho^{3/4}}\exp(-0.61/T_{11}). \tag{3}$$

The contour of X_{nuc} is also plotted in Fig. 1. At the inner side of NDAF its fraction, X_{nuc}, reaches to unity. We also calculated the flow profile of the standard accretion disk with the Keplerian angular momentum in which the fraction of free nucleons is provided through this formula, X_{nuc}. The accreting velocity of the standard disk is much less than that of NDAF, which produces the denser profile of the accretion flow for the same accretion rate, $\dot{M} = 0.1\mathrm{M}_\odot\mathrm{sec}^{-1}$. Then its ratio ϕ is very minute, $\phi \ll 0.01$. Thus it is necessary to handle the accreting matter with an appreciable abundance of heavy nuclei.

We adopt a simplified, analytical equation of state for hot, dense matter given by Lattimer & Swesty (1991), in which the heavy nuclei are treated as being in a b.c.c. lattice. In accordance with the Wigner-Seitz approximation each heavy ion is considered to be surrounded by a charge-neutral spherical cell consisting of a less dense vapor of neutrons, protons and alpha particles as well as electrons. The volume of this cell is given by $V_c = n_A^{-1}$, where n_A is the number density of heavy nuclei. We construct a three-dimensional table of the relevant thermodynamic quantities, i.e., $n_n, n_p, n_\alpha, \mu_n - \mu_p, A, Z, P_b$, as a function of the inputs (ρ, T, Y_e), where n_n, n_p, n_α are the number densities of free neutron, free proton, α particle, $\mu_n - \mu_p$ is the difference of chemical potential between the neutron and the proton, A and Z are the mean mass number and proton number of heavy nuclei. The contours of chemical potential, $\mu_n - \mu_p$, are depicted in Fig.9.

2.2 Reactions of neutrinos

The thermal and dynamical properties of a massive accretion disk are greatly influenced by neutrinos. The neutrino loss cools the disk and the interaction with ambient matter may produce the convection. In this paper the dominant neutrino reactions in the stellar core collapse are included, which are listed in Table 1. The summaries of the various neutrino cross sections of relevance in supernova theory are given in Tubbs, & Schramm (1975), Bruenn (1985) and Burrows (2001). The approximate blockings in the lepton phase space are described in Ruffert, Janka, & Schafer (1996). Here the leptons spectra are assumed to be represented by thermally equilibrium Fermi-Dirac distributions with the temperature, T (taken equal to the gas temperature), and the degeneracy factor, η_l. The neutrino cross sections, opacities, emissivities and reaction rates used in our model are listed in Table A1–5(Appendix A). When the density n_l and temperature T of leptons are given, their chemical potential μ_l is determined through the Fermi integral, $n_l(\eta_l) = 4\pi(kT/hc)^3\int_0^\infty dx x^2/[1 + exp(x - \eta_l)]$. The electron-positron pair is assumed to be in equilibrium with thermal photons.

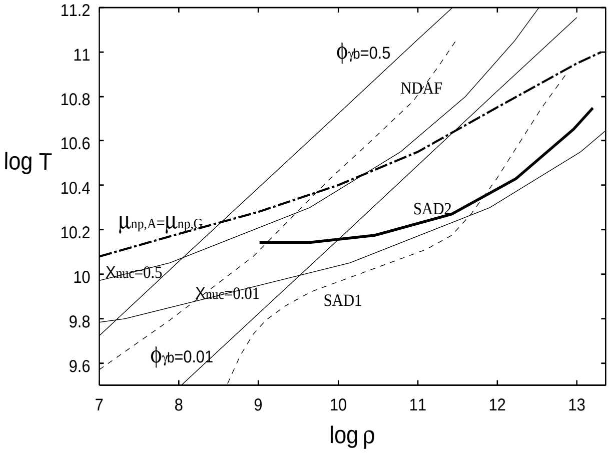

Figure 1. The loci of accreting gas on the ρ(g cm^{-3}) — T(K) plane. NDAF is the locus of the neutrino-dominant accretion flow with $\dot{M} = 0.1\mathrm{M}_\odot$ sec^{-1} and $M_{BH} = 3\mathrm{M}_\odot$. SAD1 is the locus of the standard accretion disk with Keplerian angular momentum where heavy nuclei are ignored. SAD2 is the locus of the standard accretion disk with heavy nuclei. The lines with the constant photon-to-baryon ratio $\psi_{\gamma b}$ and those with constant mass fraction of free nucleons χ_{nuc} are plotted. The phase boundary between heavy nuclei and uniform evaporated matter for the case $Y_e = 0.3$ is described by the dot-dashed line with the label $\mu_{np,A} = \mu_{np,G}$.

The reaction and transfer of neutrinos are evaluated in the simplified disk with the thickness $H(r)$ in which the matter is assumed to be homogeneously distributed in the vertical direction. The thickness $H(r)$ is taken approximately to be a scale height. The change of lepton fraction, $\dot{Y}_l$, is calculated along the accreting flow. At the inner region of the disk, the hot, dense matter changes the lepton fraction within the duration time of the matter moving along the distance Δr with the accreting velocity v_{accrt}, $\Delta t = \Delta r/v_{accrt}$. When $v_{accrt} \approx 10^{-3}c \approx 10^7$[cm/sec] and the section of the moving distance is taken to be $\Delta r \approx 0.1 r_{ms} \approx 10^5(M_{BH}/3\mathrm{M}_\odot)$[cm], the duration time is $\Delta t \approx 10$[ms]. In this time Δt the neutrino reactions do not always reach to the local thermodynamic equilibrium(LTE). The changes of leptons are calculated without LTE.

The changing rate of each lepton number in unit volume, $\dot{n}_l$, is produced through the networks of reactions,

$$\begin{aligned}
\dot{n}_e &= -\dot{n}_\beta + \dot{n}_{\bar{\beta}} - \dot{n}_A + \dot{n}^+_{URCA}, && (4)\\
\dot{n}_{e^+} &= -\dot{n}_{\bar{\beta}} - \dot{n}_{ee}, && (5)\\
\dot{n}_{\nu_e} &= \dot{n}_\beta + \dot{n}_A + \dot{n}_{ee} + \dot{n}_{NN} + \dot{n}^+_{URCA} + \dot{n}^+_\gamma, && (6)
\end{aligned}$$

Table 1. Netrino reactions

No.	Neutrino reaction	Reaction process	References
1	$e + p \rightleftharpoons \nu_e + n$	β process	Burrows(2001)
2	$e^+ + n \rightleftharpoons \bar{\nu}_e + p$	positron capture on neutron	Burrows(2001)
3	$e + A \rightleftharpoons \nu_e + A'$	electron capture on nuclei	Bruenn(1985)
4	$\nu_i + N \rightarrow \nu_i + N$	neutrino-nucleon scattering	Burrows(2001)
5	$\nu_i + A \rightarrow \nu_i + A$	neutrino-nucleus scattering	Bruenn(1985)
6	$\nu_i + e \rightarrow \nu_i + e$	neutrino electron scattering	Burrows(2001)
7	$e + e^+ \rightleftharpoons \nu_i + \bar{\nu}_i$	electron pair process	Burrows(2001)
8	$N + N \rightleftharpoons N + N + \nu_i + \bar{\nu}_i$	nucleon-nucleon bremstrahlung	Raffelt(2001)
9	$n + n \rightarrow n + p + e + \nu_e$	Urca process	Shapiro and Teukolsky(1983)
10	$\gamma \rightarrow \nu_i + \bar{\nu}_i$	plasma decay	Ruffert et al.(1996)

$$\dot{n}_{\bar{\nu}_e} = \dot{n}_{\bar{\beta}} + \dot{n}_{ee} + \dot{n}_{NN} + \dot{n}^+_\gamma, \tag{7}$$

$$\dot{n}_{\bar{\nu}_x} = \dot{n}_{ee} + \dot{n}_{NN} + \dot{n}^+_\gamma. \tag{8}$$

Here $\dot{n}_\beta, \dot{n}_{\bar{\beta}}, \dot{n}_{ee}, \dot{n}_A$ and $\dot{n}_{NN}$ are the net production rates of neutrinos by the following reactions; the β process, $e + p \rightleftharpoons \nu_e + n$, the positron capture on neutron, $e^+ + n \rightleftharpoons \bar{\nu}_e + p$, the electron pair annihilation, $e + e^+ \rightleftharpoons \nu_i + \bar{\nu}_i$, the electron capture on the nuclei, $e + A \rightleftharpoons \nu_e + A'$ and the nucleon-nucleon bremstrahlung, $N + N \rightleftharpoons N + N + \nu_i + \bar{\nu}_i$. The positive sign in these net rates indicates the increase of neutrinos. The plus sign at the upper suffix denotes the production rates of neutrinos without inverse reaction, i.e., $\dot{n}^+_{URCA}$ and $\dot{n}^+_\gamma$ are the production rates by the URCA process, $N + N \rightarrow n + p + e + \nu_e$, and by the plasma decay, $\gamma \rightarrow \nu_i + \bar{\nu}_i$.

The changes of neutrino density are also brought about by the leakage of neutrinos from the disk. The flux number density of each neutrino at the surface of the disk, $F_{n(\nu_i)}$, are approximately expressed by the production rate of neutrino, $\dot{n}^+_{\nu_i}$, and the absorptive, scattering and total opacities, $\kappa_{\nu_i a}, \kappa_{\nu_i s}$ and $\kappa_{\nu_i} = \kappa_{\nu_i a} + \kappa_{\nu_i s}$,

$$F_{n(\nu_i)} = \frac{\dot{n}^+_{\nu_i} H}{1.5\tau_{\nu_i a}\tau_{\nu_i} + \sqrt{3}\tau_{\nu_i a} + 1}, \tag{9}$$

where τ_{ν_i} and $\tau_{\nu_i a}$ are the total and absorptive optical depths for ν_i (see Appendix B). The absorptive and scattering opacities for each type of neutrino are given by

$$\kappa_{\nu_e a} = \kappa^a_\beta + \kappa^a_A + \kappa^a_{NN}, \quad \kappa_{\bar{\nu}_e a} = \kappa^a_{\bar{\beta}} + \kappa^a_{NN}, \tag{10}$$

$$\kappa_{\nu_x a} = \kappa^a_{NN}, \quad \kappa_{\nu_i s} = \kappa^s_n + \kappa^s_p + \kappa^s_A + \kappa^s_e, \tag{11}$$

where $\kappa^s_n, \kappa^s_p, \kappa^s_A$ and κ^s_e are the scattering opacities due to the scattering with neutron, proton, nucleus and electron which are represented in Table A2.

Thus the change of the each neutrino fraction, $\dot{Y}_{\nu_i}$, along the accreting flow is expressed by

$$n_b \dot{Y}_{\nu_i} = v^r \nabla_r n_{\nu_i} = \dot{n}_{\nu_i} - \frac{F_{n(\nu_i)}}{H}. \tag{12}$$

The changes of the electron fraction, $\dot{Y}_e$, and of the positron fraction, $\dot{Y}_{e^+}$, are given by

$$n_b \dot{Y}_e = \frac{\dot{n}_e}{n_b}, \quad \dot{Y}_{e^+} = \frac{\dot{n}_{e^+}}{n_b} + v^r \nabla_r \frac{n_{e^+ th}}{n_b}, \tag{13}$$

where $n_{e^+ th}$ is the number density of positrons which is equilibrium with thermal photons(see Appendix C).

The energy loss carried out by neutrinos is similarly expressed with the emissivities of neutrinos, q_{ν_i}. The emissivity of each type of neutrino is described as

$$q_{\nu_e} = q_\beta + q_{ee} + q_A + q_{NN} + q_{URCA} + q_\gamma, \tag{14}$$

$$q_{\bar{\nu}_e} = q_{\bar{\beta}} + q_{ee} + q_{NN} + q_\gamma, \tag{15}$$

$$q_{\nu_x} = q_{ee}(\nu_x) + q_{NN}(\nu_x) + q_\gamma(\nu_x), \tag{16}$$

where $q_\beta, q_{\bar{\beta}}, q_{ee}, q_A, q_{NN}, q_{URCA}$ and q_γ are emissivities by the β process, the positron capture on neutron, the electron pair annihiration, the electron capture on the nuclei, the nucleon-nucleon bremstrahlung, the URCA process, and by the plasma decay; $q_{ee}(\nu_x), q_{NN}(\nu_x), q_\gamma(\nu_x)$ are those for heavy neutrinos, $\nu_x = \nu_\mu, \nu_\tau$ (see Table A3). The energy flux density of each neutrino at the surface of the disk, $F_{\varepsilon(\nu_i)}$, is then given by

$$F_{\varepsilon(\nu_i)} = \frac{q_{\nu_i} H}{1.5\tau_{\nu_i a}\tau_{\nu_i} + \sqrt{3}\tau_{\nu_i a} + 1}. \tag{17}$$

3 RELATIVISTIC MODEL OF ACCRETION DISK WITH NEUTRINO LOSS

The duration time of GRBs requires that the collapsed, accreting matter has large specific angular momentum. The central black hole may be rapidly rotating(MacFadyen & Woosley 1999). We derive precisely the shear stress tensor $\sigma_{\varphi r}$ in Kerr spacetime. The relativistic model for the accretion disk was investigated by Novikov, & Thorne (1973). However, their model is insufficient in some respects. The boundary condition at the inner disk is not suitable, i.e., the thickness of the disk becomes infinitesimal and the density diverges to infinity at the boundary. The work produced by advection was not included in their model. We reconstruct the relativistic model without singularity and with advectional motion based on the standard theory of the thin accretion disk.

We choose units with $G = c = 1$. The metric of spacetime, in terms of Boyer-Lindquist time t and any arbitrary spatial coordinates x^j, has the form

$$ds^2 = -\alpha^2 dt^2 + g_{jk}(dx^j + \beta^j dt)(dx^k + \beta^k dt). \tag{18}$$

The metric coefficients α, β^j, g_{jk} are the lapse, shift, and 3-metric functions. Theses functions are given by

$$\alpha = \left(\frac{\Sigma\Delta}{A}\right)^{1/2}, \quad g_{rr} = \frac{\Sigma}{\Delta}, \quad g_{\theta\theta} = \Sigma, \quad g_{\varphi\varphi} = \frac{\sin^2\theta A}{\Sigma}$$

$$\beta^\varphi = -\omega = -\frac{2Mar}{A}, \quad \beta^j = g_{jk} = 0 \quad \text{for all other } j \text{ and } k,$$

where M is the mass of the black hole, a is its angular momentum per unit mass, and the functions Δ, Σ, A are defined by

$$\Delta = r^2 - 2Mr + a^2, \quad \Sigma = r^2 + a^2\cos^2\theta, \tag{19}$$
$$A = (r^2 + a^2)^2 - a^2\Delta\sin^2\theta.$$

We introduce a set of local observers who rotate with a Keplerian, circular orbit. Each observer carries an orthonormal tetrad.

For the Keplerian orbiting observer with a coordinate angular velocity of Ω, its world line is $r =$constant, $\theta =$constant, $\varphi = \Omega t +$ constant. The observer in the LNRF who rotates with the angular velocity ω measures the linear velocity of a particle moving in a Keplerian orbit as $v_{(\varphi)} = \alpha^{-1}\sqrt{g_{\varphi\varphi}}(\Omega - \omega)$. Its Lorentz factor is $\gamma = (1 - v_{(\varphi)}^2)^{-1/2}$. We adopt the Keplerian orbiting, observer's frame ("orbiting frame") with the set of it's basis vectors:

$$\begin{aligned}\mathbf{e}_{\hat{0}} &= \gamma e^{-\nu}\Big(\frac{\partial}{\partial t} + \Omega\frac{\partial}{\partial\varphi}\Big), && (20)\\ \mathbf{e}_{\hat{\varphi}} &= \gamma\Big(e^{-\psi}\frac{\partial}{\partial\varphi} + v_{(\varphi)}e^{-\nu}\big(\frac{\partial}{\partial t} + \omega\frac{\partial}{\partial\varphi}\big)\Big), && (21)\\ \mathbf{e}_{\hat{r}} &= e^{-\mu_1}\frac{\partial}{\partial r}, \quad \mathbf{e}_{\hat{\theta}} = e^{-\mu_2}\frac{\partial}{\partial\theta}, && (22)\end{aligned}$$

where $e^{\nu}, e^{\psi}, e^{\mu_1}, e^{\mu_2}$ are difined by $e^{\nu} = \alpha, e^{2\psi} = g_{\varphi\varphi}, e^{2\mu_1} = g_{rr}, e^{2\mu_2} = g_{\theta\theta}$.

The corresponding orthogonal basis of one-forms is

$$\vec{\omega}^{\hat{t}} = \hat{\alpha}\mathbf{d}t - v_{(\varphi)}\gamma e^{\psi}\mathbf{d}\varphi, \quad \vec{\omega}^{\hat{\varphi}} = -\Omega\gamma e^{\psi}\mathbf{d}t + \gamma e^{\psi}\mathbf{d}\varphi$$
$$\vec{\omega}^{\hat{r}} = e^{\mu_1}\mathbf{d}r, \quad \vec{\omega}^{\hat{\theta}} = e^{\mu_2}\mathbf{d}\theta, \qquad (23)$$

where $\hat{\alpha}$ is the "lapse function" in an orbital frame, $\hat{\alpha} = \alpha\gamma(1 + v_\omega v_{(\varphi)})$.

The shear stress in an orbital frame is expressed by

$$\sigma^{\hat{r}\hat{\varphi}} = e^{\hat{r}}_{\alpha}e^{\hat{\varphi}}_{\beta}\sigma^{\alpha\beta}, \qquad (24)$$

where $\sigma^{\alpha\beta}$ is the shear stresses in the Boyer-Lindquist coordinate, and $e^{\hat{a}}_{\alpha}$ is the Boyer-Lindquist components of the basis of one-forms (23) in orbital frame, $\vec{\omega}^{\hat{a}} = e^{\hat{a}}_{\alpha}\mathbf{d}x^{\alpha}$. The shear stress in the Boyer-Lindquist coordinate is defined by

$$\sigma_{\alpha\beta} \equiv \frac{1}{2}(u_{\alpha;\mu}h^{\mu}_{\beta} + u_{\beta;\mu}h^{\mu}_{\alpha}), \qquad (25)$$

where $h_{\mu\nu}$ is the projection tensor, $h_{\mu\nu} = g_{\mu\nu} + u_\mu u_\nu$. The shear stress in the orbiting frame is then represented as

$$\sigma^{\hat{r}\hat{\varphi}} = \frac{1}{2}\Big\{\frac{1}{\sqrt{g_{rr}}}(\gamma^2 v_{(\varphi)}\frac{\partial\ln(\Omega - \omega)}{\partial r} + \frac{1}{2}v_\omega\frac{\partial\ln\omega}{\partial r})\Big\}, \qquad (26)$$

where v_ω is the rotating velocity of spacetime, $v_\omega = \alpha^{-1}\sqrt{g_{\varphi\varphi}}\omega$. While the absolute value of the shear stress in the Shwarzchield spacetime monotonously increases as $|\sigma^{\hat{r}\hat{\varphi}}| \approx 0.75\Omega$ according to $r \to r_{ms}$, the shear stress in rapidly rotating spacetime has the minimum in the vicinity of r_{ms}.

The generation rate of the viscous heating is evaluated in the orbiting frame by

$$\dot{\epsilon} = -t_{\hat{i}\hat{j}}\sigma^{\hat{i}\hat{j}}, \qquad (27)$$

where $t_{\hat{i}\hat{j}}$ is the stress tensor. For the "α model" of the viscosity the stress tensor is expressed by $t_{\hat{i}\hat{\varphi}} = \alpha_{vis}P_{th}$, where P_{th} is the thermal pressure and α_{vis} is a parameter with $\alpha_{vis} = 0.1 - 0.01$.

Then we consider the energy equation in the orbiting frame. The energy-momentum tensor of the viscous fluid with heat flux is expressed(Misner, Thone & Wheeler 1973; Novikov, & Thorne 1973; Yokosawa 1995) as follows,

$$T^{\hat{\alpha}\hat{\beta}} = (\rho + \epsilon)u^{\hat{\alpha}}u^{\hat{\beta}} + Ph^{\hat{\alpha}\hat{\beta}} + t^{\hat{\alpha}\hat{\beta}} + q^{\hat{\alpha}}u^{\hat{\beta}} + u^{\hat{\alpha}}q^{\hat{\beta}}, \qquad (28)$$

where ρ, ϵ, and P are the rest-mass density, internal energy density and pressure and $q^{\hat{\alpha}}$ is the heat flux carried by neutrinos and photons. By using the covariant derivative, $\vec{\nabla}$, the local energy conservation, $\vec{u} \cdot (\vec{\nabla} \cdot \mathbf{T}) = 0$, is represented as

$$\frac{\partial\epsilon u^{\hat{0}} + q^{\hat{0}}}{\partial x^{\hat{0}}} + \frac{1}{\hat{\alpha}}\nabla_{\hat{i}} \cdot \hat{\alpha}(\epsilon u^{\hat{i}} + q^{\hat{i}}) + P\frac{\partial u^{\hat{0}}}{\partial x^{\hat{0}}} \qquad (29)$$
$$+\frac{P}{\hat{\alpha}}\nabla_{\hat{i}} \cdot \hat{\alpha}u^{\hat{i}} + \sigma^{\hat{\alpha}\hat{\beta}}t_{\hat{\alpha}\hat{\beta}} = 0. \qquad (30)$$

The mass conservation $\vec{\nabla} \cdot (\rho\vec{u}) = 0$ is written by

$$\frac{\partial\rho u^{\hat{0}}}{\partial x^{\hat{0}}} + \frac{1}{\hat{\alpha}}\nabla_{\hat{i}}\hat{\alpha}\rho u^{\hat{i}} = 0. \qquad (31)$$

By using the projection vector in φ direction, $\mathbf{h}^{\varphi} = h^{\varphi\beta}$, the Euler equation in the φ direction, $\mathbf{h}^{\varphi} \cdot (\nabla \cdot \mathbf{T}) = 0$, is expressed in the frame fixed at the distant stars,

$$\frac{\partial(\rho + \epsilon + p)u^0u_\varphi}{\partial t} + \frac{1}{\alpha}\nabla_i\Big(\alpha(\rho + \epsilon + P)u^iu_\varphi + t^i_\varphi + u_\varphi q^i\Big) \qquad (32)$$
$$+\frac{\partial\alpha p}{\alpha\partial x^\varphi} = 0. \qquad (33)$$

We are interesting in the gross properties of the disk with neutrino loss. For simplicity, we consider a steady state disk with axially symmetry. As in the standard theory of thin accretion disks, we consider height-averaged quantities. Putting the integrated stress as $W = \int_{-h}^{h} t_{\hat{r}\hat{\varphi}}dz = \int_{-h}^{h} \alpha_{vis}P_{th}dz$, and introducing the flux density at the surface of the disk, $F = q^{\hat{z}}(z = H)$, the energy equation is expressed by

$$F + \Big(\sigma_{\hat{r}\hat{\varphi}} + \frac{1}{\hat{\alpha}\alpha_{vis}}(\nabla_{\hat{r}}\hat{\alpha}u^{\hat{r}} + P^{-1}\nabla_{\hat{r}}\hat{\alpha}\epsilon u^{\hat{r}})\Big)W = 0. \qquad (34)$$

From the equation (33) the conservation of angular momentum is

$$\nabla_i \cdot \Big(\alpha(\rho + \epsilon + P)u^iu_\varphi + t^i_\varphi + u_\varphi q^i\Big) = 0 \qquad (35)$$

The angular momentum is transported by the viscous stress t^i_φ and by the neutrino flowing q^i. Introducing the total mass flux $\dot{M}$, we express the transport equation of angular momentum as

$$\frac{\partial}{\partial r}\big(-\frac{\dot{M}}{2\pi}u_\varphi + \sqrt{\Delta}\gamma e^{\psi}W\big) - 2ru_\varphi F = 0. \qquad (36)$$

It has the solution:

$$W = \frac{\dot{M}}{2\pi}\Omega\Pi, \qquad (37)$$

where Π is the function with the value of unity at the great distance from the hole:

$$\Pi = \frac{u_\varphi + C}{\sqrt{\Delta}\gamma e^{\psi}\Omega} + \frac{2\pi fg}{\Omega\dot{M}}. \qquad (38)$$

The term fg is due to the neutrino flowing. The functions f and g are

$$\begin{aligned}f &= -\frac{\dot{M}}{2\pi}\int_r^\infty \frac{2\varpi u_\varphi\tilde{\sigma}_{\hat{r}\hat{\varpi}}}{g\Delta\gamma^2e^{2\psi}}(u_\varphi + C)d\varpi, && (39)\\ g &= \frac{1}{\sqrt{\Delta}\gamma e^{\psi}}\exp\Big[-\int_r^\infty \frac{2\varpi u_\varphi\tilde{\sigma}_{\hat{r}\hat{\varphi}}}{\sqrt{\Delta}\gamma e^{\psi}}d\varpi\Big], && (40)\\ \tilde{\sigma}_{\hat{r}\hat{\varphi}} &= \sigma_{\hat{r}\hat{\varphi}}\Big(1 + (1 + \frac{\epsilon}{P})\frac{\sqrt{\Delta}u^{\hat{r}}}{2\sigma_{\hat{r}\hat{\varphi}}\alpha_{vis}\varpi^2}(\frac{\partial\ln\sqrt{\Delta}u^{\hat{r}}}{\partial\varpi} && (41)\\ &+ \frac{1}{1 + P/\epsilon}\frac{\partial\ln\epsilon}{\partial\varpi})\Big). && (42)\end{aligned}$$

Here C is the integral constant. Novikov & Thorne(1973) adopted such as $C = -u_\varphi(r_{ms})$ since they assumed no viscous stress can act at $r = r_{ms}$. The accreting matter with viscosity continuously flows into a black hole through the boundary radius r_{ms}(Yokosawa 1995). We set the constant C so that the accreting matter continuously flows through the radius r_{ms} and then the viscous stress has the value such as $t_{\hat{r}\hat{\varphi}}(r_{ms}) = \alpha_{vis} p(r_{ms})$,

$$C = -u_\varphi(r_{ms}) + \frac{4\pi h}{\dot{M}}\sqrt{\Delta(r_{ms})}\gamma(r_{ms})e^{\psi}(r_{ms})\alpha_{vis}P(r_{ms}). \quad (43)$$

Dynamically equilibrium structure of the disk is given by the Euler equation. The equation of motion of the fluid, $h_i^k T^j_{k;j} = 0$, for the steady, axially symmetric and rotating fluid can be expressed in the total differential form:

$$\frac{dp}{\rho + P} = \gamma^2(-d\nu + v^2_{(\varphi)}d\psi - v_{(\varphi)}v_\omega d\ln\omega) \equiv -dU. \quad (44)$$

The equipressure surfaces are given by the equation U =constant. The quantity $U = U(p)$ is equal in the Newtonian limit to the total potential (gravitational plus centrifugal) expressed in the units of c^2 (Abramowicz, Jaroszyński Sikora 1978). In the neighborhood of equatorial plane the potential U is expanded with z:

$$U = U_0(r, 0) + \frac{1}{2}\Omega_0^2 z^2, \quad (45)$$

where Ω_0^2 is

$$\Omega_0^2 = \frac{\mathrm{G}M}{r^3}\Phi(r). \quad (46)$$

The function $\Phi(r)$ becomes unity far a way from a hole. Its explicit expression of $\Phi(r)$ is shown in Appendix D. The thickness of the disk is approximately given by the scale height,

$$H = \sqrt{2\frac{P}{\rho}}\Omega_0^{-1}. \quad (47)$$

The energy equation (34) integrated over the thickness of the disk is represented with the mass accretion rate, $\dot{M} = -4\pi r H\rho\hat{\alpha}u^{\hat{r}}$,

$$F + \sigma_{\hat{r}\hat{\varphi}}W + \frac{\dot{M}}{4\pi r^2}\Big(\frac{\partial}{\partial\ln r}\frac{\epsilon + P}{\rho} - \frac{P}{\rho}\frac{\partial\ln P}{\partial\ln r}\Big) = 0 \quad (48)$$

The flux density F is evaluated by the simplified neutrino transfer,

$$F = \sum_{\nu_i}\frac{q_{\nu_i}H}{1.5\tau_{\nu_i a}\tau_{\nu_i} + \sqrt{3}\tau_{\nu_i a} + 1}, \quad (49)$$

where ν_i means the flaver of neutrino, $\nu_i = \nu_e, \bar{\nu}_e, \nu_\mu, \bar{\nu}_\mu, \nu_\tau, \bar{\nu}_\tau$. Thus the basic equations (48) and (37) determine the stationary, thermally equilibrium structure of accretion disk.

In addition to the above formalism of accretion disk, we shall consider the thermal energy of the partially degenerated matter which contributes to the viscous heating and the advection. In the ranges of density and temperature, $10^{11} < \rho < 10^{13}$(g/cm^3) and $10^{10} < T < 10^{11}$(K), the degeneracy factors of electrons has the values in the range, $5 < \eta_e < 15$ (see Fig. 10). The pressure and the internal energy of electrons are expressed as

$$\begin{aligned} P_e &= \frac{\mu_e}{12\pi^2}\left(\frac{\mu_e}{\hbar c}\right)^3\left[1 + \left(\frac{kT}{\mu_e}\right)^2\left(2\pi^2 - 3\left(\frac{m_e c^2}{kT}\right)^2\right)\right. \\ &+ \left.\left(\frac{kT}{\mu_e}\right)^4\pi^2\left(\frac{7}{15}\pi^2 - \frac{1}{2}\left(\frac{m_e c^2}{kT}\right)^2\right)\right], \quad (50) \\ \epsilon_e &= \frac{\mu_e}{4\pi^2}\left(\frac{\mu_e}{\hbar c}\right)^3\left[1 + \left(\frac{kT}{\mu_e}\right)^2\left(2\pi^2 - \left(\frac{m_e c^2}{kT}\right)^2\right)\right. \\ &+ \left.\left(\frac{kT}{\mu_e}\right)^4\left(\frac{7}{15}\pi^2 - \frac{1}{2}\left(\frac{m_e c^2}{kT}\right)^2\right)\right]. \quad (51) \end{aligned}$$

The first terms in the both square brackets provide the pressure and internal energy corresponding to the completely degenerated state. The second and third terms depend on the temperature. We introduce the thermal pressure of electrons, P_{eth}, expressed by the above expression without the first term. The completely degenerate matter has no contribution in cooling or heating by advectional motion. Thus the pressure and internal energy density without the completely degenerate parts are used for the advection or for the α model of viscosity.

The baryonic matter is hardly degenerated over the above phase area in ρ — T plane. The pressure of baryonic matter is consist of that of free nucleons P_{nuc}, that of α particles P_α, that of heavy nuclei (Lattimer & Swesty 1991),

$$P_b = P_{nuc} + P_\alpha - \beta(D - uD') + \frac{un_A}{A}h[kT(1-u) - \mu_A u], \quad (52)$$

where μ_H is the chemical potential of heavy nuclei, u is the fraction of space occupied by heavy nuclei, β, D, D', h are the functions of nuclear quantities (Lattimer & Swesty 1991). The values of P_b in the above phase area are almost same as $n_b kT$. Thus the internal energy of baryonic matter is approximately set to be $\epsilon_b \approx 3/2P_b$. The total pressure and internal energy density are given by

$$\begin{aligned} P &= P_b + P_e + aT^4(\frac{11}{12} + \frac{7}{8}\tau), \quad (53) \\ \epsilon &= \epsilon_b + \epsilon_e + aT^4(\frac{11}{4} + \frac{21}{8}\tau), \quad (54) \end{aligned}$$

where a is the radiation constant τ is the neutrino opacity, $\tau = \Sigma(\tau_{\nu_i}/2 + 1/\sqrt{3})/(\tau_{\nu_i}/2 + 1/\sqrt{3} + 1/3\tau_{\nu_i a})$. The third terms on the right hand side represent the contributions of radiation in thermally equilibrium with relativistic electron positron pairs and of neutrinos(Popham, & Narayan 1995)

4 RESULTS

We have solved the stationary flow structure at the position range, $r = r_{ms} \sim 10^2 r_{ms}$. At the outer boundary of the calculation we select the most large value of Y_e within $Y_e \leqslant 0.5$ which satisfies the stationary conditions, (48) and (37). The fractions of neutrinos at the boundary, Y_{ν_i}, are taken which provide the local thermodynamical equilibrium in neutrino reactions. The accretion rate $\dot{M}$ is taken to be $\dot{M} = 0.01 \sim 1\mathrm{M}_\odot\mathrm{sec}^{-1}$, and the angular momentum parameter of a black hole ranges from $a = 0 \sim 1$. The accreting velocity, $v \equiv u^r/u^0$, is derived from the mass conservation, $\dot{M} = const.$, for given density ρ and height H. The typical parameters in the models of GRBs are selected as $a = 0.9$, $\dot{M} = 0.1\mathrm{M}_\odot\mathrm{sec}^{-1}$, and $M_{BH} = 3\mathrm{M}_\odot$(MacFadyen & Woosley 1999). The viscous parameter is set to be $\alpha_{vis} = 0.05$(Turner 2004).

4.1 Flow structures

The flow profiles are shown in Fig. 2, where the density ρ, temperature T, accreting velocity v and scale height H are plotted in the radius normalized by the gravitational radius, $r_* = r/r_g$. While the density ρ increases according to the accretion rate $\dot{M}$ and reaches to a very high value, $\rho \geqslant 10^{13}$[g/cm^3] for $\dot{M} \geqslant 0.1\mathrm{M}_\odot\mathrm{sec}^{-1}$, the temperature, scale height and accreting velocity are little changed for the wide range of accretion rate, $\dot{M} = 10^{-2} \sim 1\mathrm{M}_\odot\mathrm{sec}^{-1}$. The profiles of temperature and accreting velocity are nearly constant along the flow, $T \approx 3 \times 10^{10}$K and $v \approx 10^{-3}c$. The scale height is expressed as $H \approx 0.1r_g(r_*)^{5/4}$, showing the very thin disk formed around a black hole.

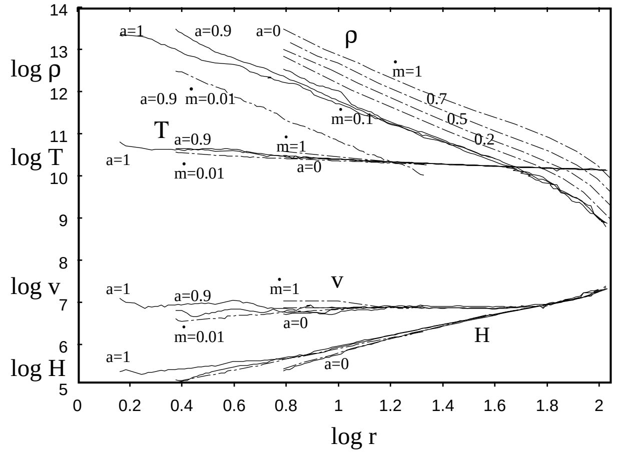

Figure 2. The flow profiles of density ρ(g cm^{-3}), temperature T(K), drift velocity v(cm/sec), scale hight H(cm). The radius r is normalized by the gravitational radius r_g. The mass of a black hole is fixed to be $M_{BH} = 3\mathrm{M}_\odot$, and the angular momentum parameters are selected such as $a = 0, 0.9, 1$. The numbers denote the accretion rates, $\dot{M}$= 1,0.5,0.2,0.1,0.01(M$_\odot$ sec^{-1}). The flow profiles with $\dot{M} = 0.1\mathrm{M}_\odot\mathrm{sec}^{-1}$ are plotted by filled lines, and those with $\dot{M} = 1\mathrm{M}_\odot\mathrm{sec}^{-1}$ and $\dot{M} = 10^{-2}\mathrm{M}_\odot\mathrm{sec}^{-1}$ are depicted by dot-dashed lines.

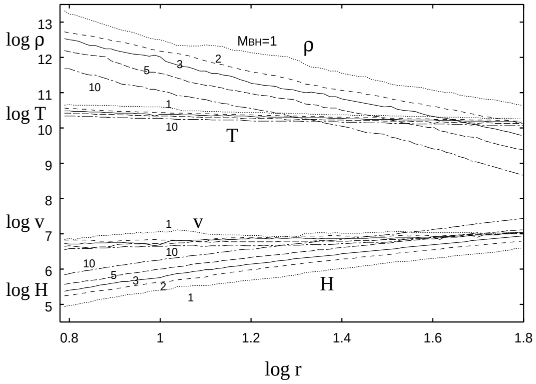

Figure 3. The same as Fig. 2, but for the mass dependence of a black hole. The numbers denote the masses of a black hole, M_{BH}= 1,2,3,5,10(M$_\odot$). The accretion rate and the specific anguler momentum of a black hole are fixed as $\dot{M} = 0.1\mathrm{M}_\odot\mathrm{sec}^{-1}$ and a=0. The radius r is normalized by the gravitational radius r_g.

These flow profiles are somewhat different from the previous works on the advection dominant flow with neutrino loss(Popham, Woosley & Fryer 1999; Narayan, Piran, & Kumar 2001; Di Matteo, Perna, & Narayan 2002). In the previous cases the temperature increases in proportion to the accretion rate. The profiles of the temperature and velocity rapidly increase to be $T \geqslant 10^{11}$K and $v \rightarrow c$ for $r \rightarrow r_{ms}$. Then the density does not reach to the extremly high value which is restricted to be $\rho \approx 10^{10\sim 12}[\mathrm{g/cm}^3]$ in the ranges of accretion rate, $\dot{m} = 0.1 \sim 10M_\odot$/sec. These differences in our results and previous ones are caused mainly by the cooling process, which will be discussed later. In the previous cases the most of neutrinos are absorbed by free nucleons and thus trapped in the accreting flow. In our study the anti-electron neutrinos $\bar{\nu}_e$ are little absorbed by free protons since free protons are reduced in the fraction, $Y_p \leqslant 10^{-3}$. The accretion disk is then efficiently cooled by $\bar{\nu}_e$. It suppresses the rise of temperature and velocity, which then produces the highly dense flows.

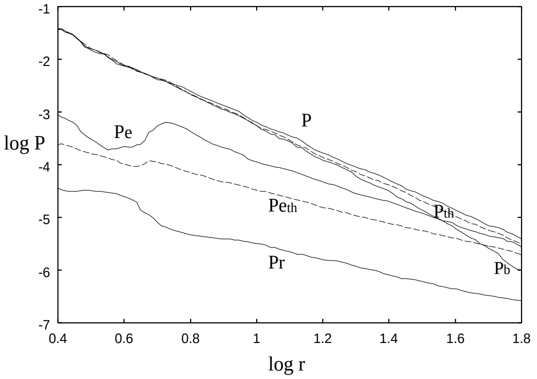

Figure 4. The profiles of total pressure P, electron pressure P_e, pressure of baryonic matter P_b, radiation pressure P_r, total thermal pressure P_{th}, and the thermal pressure of electrons P_{eth} are plotted in the case of the accretion with $\dot{M} = 0.1\mathrm{M}_\odot$ sec^{-1}, $M_{BH} = 3\mathrm{M}_\odot$ and $a = 0.9$. The unit of pressure P is (MeVfm^{-3}).

The density ρ and the temperatute T decrease as the mass of a central black hole increases when the accretion rate is restricted to be constant. The flow profiles are shown in Fig. 3 where the mass M_{BH} is changed from $1\mathrm{M}_\odot$ to $10\mathrm{M}_\odot$ and other parameters are fixed to be $a = 0, \quad \dot{M} = 0.1\mathrm{M}_\odot\mathrm{sec}^{-1}$. Their scale dependences are described approximately as $T \propto M_{BH}^{-1/3}$, $H \propto M_{BH}$ and $\rho \propto \dot{M}M_{BH}^{-2}$. That of the surface density is then $\Sigma = \rho H \propto M_{BH}^{-1}\dot{M}$. Thus the obtained flow profiles are expressed approximately by $\rho \approx 2 \times 10^{14} r_*^{-2.5}\dot{m}m^{-2}[\mathrm{g/cm}^3]$ and $T \approx 5 \times 10^{10} r_*^{-1/4} m^{-1/3}$K, where m is the mass of a central black hole normalized by $1\mathrm{M}_\odot$ and $\dot{m}$ is the accretion rate normalized by $1\mathrm{M}_\odot$/sec.

The inner disk is supported mainly by the baryon pressure P_b. The compositions of the pressure, P_b, P_e, P_r and the thermal pressure, $P_{th}, P_{e,th}$ are shown in Fig. 4. While the electron pressure P_e dominates at the outer region, $r \geqslant 15r_{ms}$, it more gradually increases than P_b according to the accreting flow. When Y_e rapidly decreases, the electron pressure itself decreases along the flow. The contribution of the radiation pressure to the total pressure is negligibly small at the inner region, but at the outer region, $r \geqslant 10^2 r_g$, it becomes comparable with that of P_b. The thermal pressure of electrons P_{eth} is comparable with its degenerate part of the pressure. The degeneracy factor of electron η_e is ranged as $\eta_e \approx 2 \sim 10$ for $\dot{m} = 0.1$ which doesn't reach to an extremely large value(see Fig. 10).

4.2 Composition and chemical potential

The composition of accreting matter which consists of free neutrino, free proton, electron, positron, and each flavor type of neutrino is shown in Fig. 5 – 8. The massive accretion rates, $\dot{M} = 0.05 \sim 1\mathrm{M}_\odot\mathrm{sec}^{-1}$ for $a = 0$, are selected in Fig. 5 and Fig. 6, while the less ones, $\dot{M} = 0.005 \sim 0.1\mathrm{M}_\odot\mathrm{sec}^{-1}$ for $a = 0.9$, are shown in Fig. 7 and Fig. 8. The fraction of free neutron Y_n increases along the accreting flow and reaches to a dominant value at the inner side of the disk, $Y_n \approx 0.7 \sim 0.8$. However the fraction of free proton decreases along the flow and reduces to an extremely small value, $Y_p \approx 10^{-3\sim -4}$. When the accretion rate $\dot{m}$ increases, the proton fraction decreases as, $Y_p \propto \dot{m}^{-1}$ though the fraction of neutron remains a constant value at the inner side of the disk, $Y_n \approx 0.7 \sim 0.8$. The number ratio of free neutron to free proton, n_n/n_p, is proportional to the degeneracy factor,

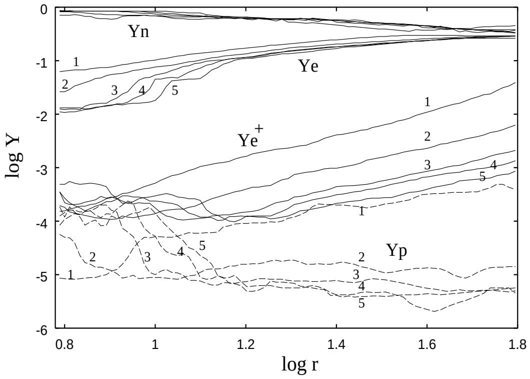

Figure 5. The profiles of electron fraction Y_e, positron fraction Y_{e^+}, free neutron fraction Y_n, and free proton fraction Y_p for the accretion onto a non-rotating black hole, $a = 0$, with mass $M_{BH} = 3\mathrm{M}_\odot$. The numbers of the label 1,2,3,4,5 denote the cases for accretion rates, $\dot{M}$ = 0.05,0.2,0.5,0.7,1($\mathrm{M}_\odot$ sec^{-1}). The radius r is normalized by the gravitational radius r_g.

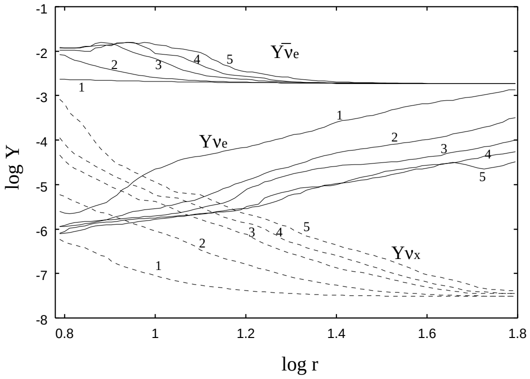

Figure 6. The profiles of of electron neutrino Y_{ν_e}, electron anti-neutrino $Y_{\bar{\nu}_e}$, heavy neutrino Y_{ν_x}. Others are same as Fig.5.

$\eta_{np} = (\mu_n - \mu_p)/kT$, i.e., $n_n/n_p \approx \exp(\eta_{np})$. The locus of accreting matter in the $\rho - T$ plane is traced to the increase of chemical potential of $\mu_n - \mu_p$ (see Fig. 9). The larger accretion rate moves the locus into the larger potential in $\mu_n - \mu_p$. In the typical case of the accretion its factor η_{np} increases from 5 at the outer boundary of the disk to 12 at the inner side of the disk (see Fig. 10). The accretion flow with large efficiency of neutrino loss produces the locus with relatively low temperature in the $\rho - T$ plane, $T \approx 2 \sim 5 \times 10^{10}$ K, which means that the larger accretion flow has the larger number ratio, n_n/n_p. These larger number ratios, $n_n/n_p \approx 10^{3\sim4}$, result in the larger differences in the composition and opacity between ν_e and $\bar{\nu}_e$.

The high dense matter and the sufficient time of reaction proceed the electron capture on a proton. The electron fraction Y_e gradually decreases along the flow. The fraction of electron neutrinos, Y_{ν_e}, rapidly decreases along the accretion flow, while the fraction of antielectron neutrinos, $Y_{\bar{\nu}_e}$, gradually increases. These fraction changes are brought about mainly through the following reactions:

$$e + p \rightleftharpoons \nu_e + n, \tag{55}$$

$$e^+ + n \rightleftharpoons \bar{\nu}_e + p, \tag{56}$$

$$e + e^+ \rightleftharpoons \nu_e + \bar{\nu}_e \tag{57}$$

The fraction of heavy neutrinos Y_{ν_x} increases along the flow due to the reactions, $e + e^+ \rightleftharpoons \nu_i + \bar{\nu}_i$ and $N + N \rightleftharpoons N + N + \nu_i + \bar{\nu}_i$. In some cases, $\dot{m} \geqslant 0.05$ for $a = 0.9$, it exceeds that of ν_e at the inner side of disk, $Y_{\nu_x} \geqslant Y_{\nu_e}$. The neutralization of the matter is remarkable, $Y_e \leqslant 0.03$ for $\dot{m} \geqslant 0.02$, near the inside boundary, $r \approx r_{ms}$, where the equation of state for dense, hot matter drastically changes. The composition of the accreting matter then rapidly changes.

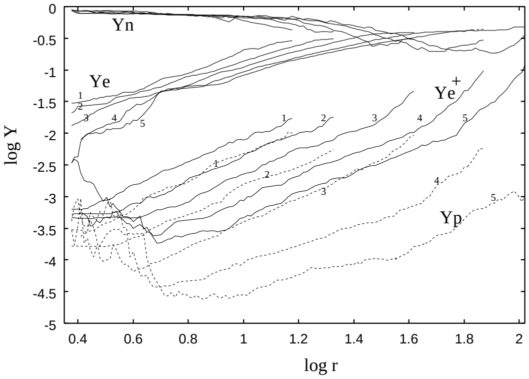

Figure 7. The same as Fig.5, but for the cases of less accretion rates with $a = 0.9$ and $M_{BH} = 3\mathrm{M}_\odot$. The numbers of the label 1,2,3,4,5 denote the cases for accretion rates, $\dot{M} =$ 0.005,0.01,0.02,0.05,0.1($\mathrm{M}_\odot$ sec^{-1}).

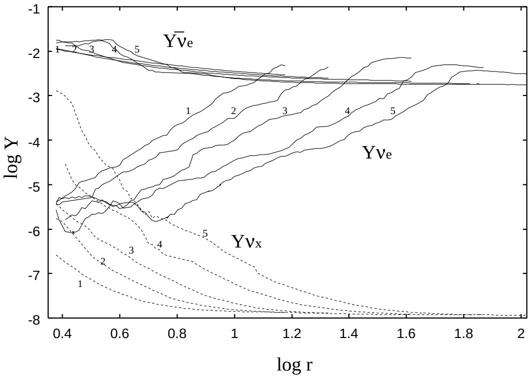

Figure 8. The same as Fig.6, but for a rotating black hole with $a = 0.9$. The numbers of the label 1,2,3,4,5 are same as in Fig. 7.

4.3 Emissivities and opacities of neutrinos

Let's evaluate the emissivities of neutrinos produced by the accretion. The emissivities by various types of reactions are shown in Fig. 11, in the typical case of the accretion. The most efficient emissivity is produced by the positron capture on neutron, $e^+ + n \rightarrow \bar{\nu}_e + p$. At the outer side, $r \geqslant 20 r_{ms}$, the pair production, $e + e^+ \rightarrow \nu_e + \bar{\nu}_e$ and the nuclei reaction, $e + A \rightarrow \nu_e + A'$, also contribute to the total emissivity. At the inner side of the disk the URCA process and nucleon—nucleon bremstrahlung become efficient. Though the emissivity by antielectron neutrinos $q_{\bar{\nu}_e}$ is dominant, the other type of neutrinos, ν_e, ν_x, also produce some efficient emissivities. The emissivity by heavy neutrinos, q_{ν_x}, becomes comparable with $q_{\bar{\nu}_e}$ near the inner boundary, $q_{\bar{\nu}_e} \approx q_{\nu_x} \approx 10^{34}$(erg/cm^3/sec). The emissivity increases sharply along the flow and the total emissivity is expressed approximately as $q = q_{\bar{\nu}_e} + q_{\nu_e} + q_{\nu_x} \approx 10^{36} r_*^{-4.25}$(erg/cm^3/sec).

The opacities of absorption and scattering for each type of

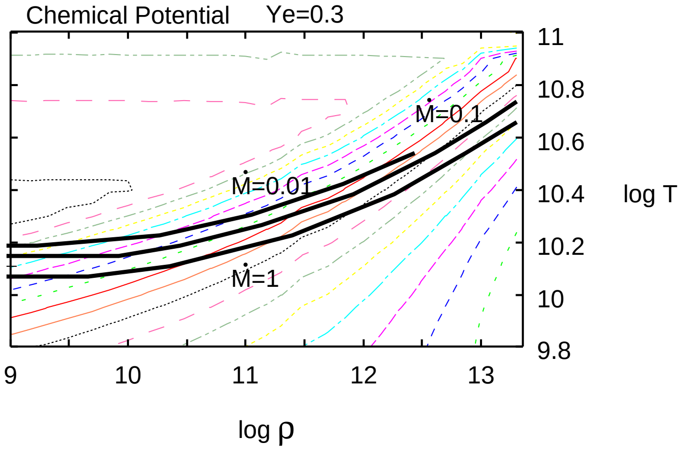

Figure 9. The loci of accreting gas for the accretion rate $\dot{M} = 0.01, 0.1, 1(\mathrm{M}_\odot\ \mathrm{sec}^{-1})$ on the $\rho(\mathrm{g\ cm}^{-}3)$ — $T(\mathrm{K})$ plane. The contours of chemical potential $\mu_n - \mu_p$ with constant electron fraction $Y_e = 0.3$ are also plotted.

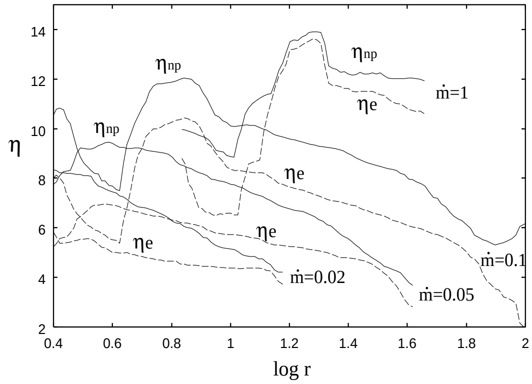

Figure 10. The profiles of degeneracy factors for η_{np} and η_e. The profiles denoted by the accretion rates $\dot{m}$=0.1, 0.05, 0.02($\mathrm{M}_\odot \mathrm{sec}^{-1}$) are shown, where $a = 0.9$, and those by $\dot{m} = 1(\mathrm{M}_\odot \mathrm{sec}^{-1})$ are in the case with $a = 0$. The mass of a black hole is set to be $M_{BH} = 3\mathrm{M}_\odot$.

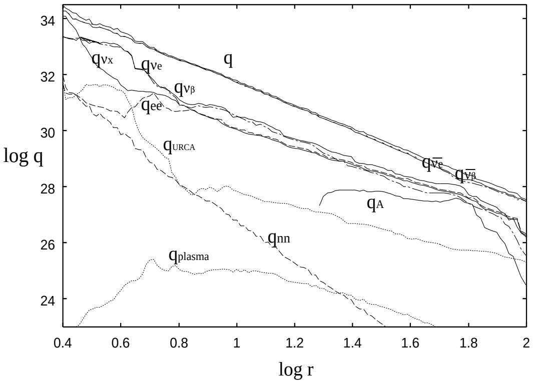

Figure 11. The profile of total emissivity of neutrinos q and those of antielectron neutrinos $q_{\bar{\nu}_e}$, electron neutrinos q_{ν_e}, heavy neutrinos q_{ν_x} are plotted in the case of the accretion with $M_{BH} = 3\mathrm{M}_\odot, a = 0.9$, and $\dot{M} = 0.1\mathrm{M}_\odot$/sec. The emissivities by β process q_β, positron capture on neutron q_{e^+n}, e^-, e^+ pair annihilation q_{ee}, URCA process q_{URCA}, nucleon-nucleon bremsstrahlung q_{nn}, plasma process q_{plasma}, and nucleus reaction q_A are also depicted. The unit of emissivity q is (erg cm^{-3}sec^{-1}).

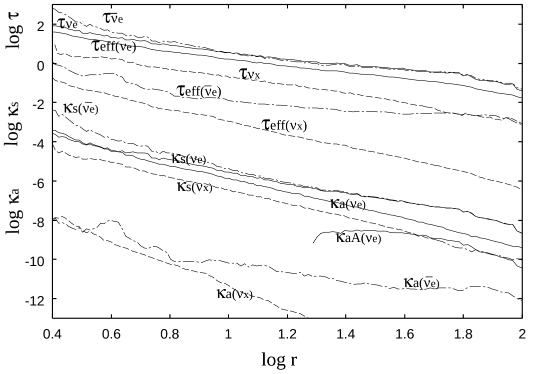

Figure 12. The profiles of absorption opacity $\kappa_a(\nu_I)$, scattering opacity $\kappa_s(\nu_i)$, effective optical depth $\tau_{eff}(\nu_i)$, and total optical depth τ_{ν_i}, for $\nu_i = \nu_e, \nu_e, \nu_x$, are plotted. The neutrino-nucleus opacity is labeled by κ_{aA}. The unit of opacity κ is (cm^{-1}). The parameters of accretion are same as in Fig. 11.

neutrinos are shown in Fig. 12. The absorption opacity of ν_e is very much larger than those of $\bar{\nu}_e$, ν_x; $\kappa_a(\nu_e) \gg \kappa_a(\bar{\nu}_e) \geqslant \kappa_a(\nu_x)$. The electron neutrino ν_e is absorbed mainly by dense free neutrons through the reaction, $\nu_e + n \rightarrow e + p$, while the antielectron neutrino $\bar{\nu}_e$ is little absorbed by rare free protons, $\bar{\nu}_e + p \rightarrow e^+ + n$. The scattering opacities of $\bar{\nu}_e$ and ν_e are comparable except near the inside boundary where the chemical potential of $\bar{\nu}_e$ is to some extent larger than that of ν_e, $\eta_{\bar{\nu}_e} > \eta_{\nu_e}$, which brings about the larger scattering opacity of $\bar{\nu}_e$(see Table A2). The both total optical depths of $\bar{\nu}_e$ and ν_e, are very large with same order of magnitude at the inside of the disk, $\tau_{\bar{\nu}_e} = \tau_{\bar{\nu}_e a} + \tau_{\bar{\nu}_e s} \geqslant \tau_{\nu_e} = \tau_{\nu_e a} + \tau_{\nu_e s} \sim 10^2$. However, the difference of effective optical depth between $\tau_{\bar{\nu}_e}^{eff}$ and $\tau_{\nu_e}^{eff}$ is remarkable, i.e., $\tau_{\nu_e}^{eff}(\geqslant 30) \gg \tau_{\bar{\nu}_e}^{eff}(\leqslant 1)$, where the effective optical depth is defined by $\tau_{\nu_i}^{eff} = \sqrt{\tau_{\nu_i}^a \tau_{\nu_i}^s}$. Most of ν_e are absorbed in the disk and their energy is deposited in the accreting matter. On the other hand the antielectron neutrinos $\bar{\nu}_e$ carry out the thermal energy from the disk to the outer atmosphere. The effective optical depth of ν_e is approximately described as $\tau_{\nu_e}^{eff} \approx 6 \times 10^3 r_*^{-2}(m)^{-1}\dot{m}$. It becomes over unity at the radius, $r \leqslant 14 r_g(M_{BH}/3\mathrm{M}_\odot)^{-1/2}(\dot{M}/(0.1\mathrm{M}_\odot/\mathrm{sec}))^{1/2}$, where the electron neutrino sphere(disk) is formed. The sphere of antielectron neutrinos or that of heavy neutrinos are not formed when $\dot{m} \leqslant 0.1$. The total optical depths of $\bar{\nu}_e$ and ν_e become over unity, $\tau_{\nu_e}, \tau_{\bar{\nu}_e} \geqslant 1$, where $r \leqslant 24 r_g(M_{BH}/3\mathrm{M}_\odot)^{-1/2}(\dot{M}/(0.1\mathrm{M}_\odot/\mathrm{sec}))^{1/2}$.

The flux densities of neutrinos, $F_{\nu_i}(r)$, are shown in Fig. 11. The flux density of electron neutrinos, F_{ν_e}, doesn't increase along the accreting flow. The ratio of the flux density of $\bar{\nu}_e$ to that of ν_e becomes large to be $F_{\bar{\nu}_e}/F_{\nu_e} \approx 10^{3\sim4}$ at the inside of the disk. The very large difference between $F_{\bar{\nu}_e}$ and F_{ν_e} seriously restricts the efficiency of the annihiration of ν_e and $\bar{\nu}_e$ at the outside of the disk, which results in the difficulty in the formation of a fire ball by the annihiration of $\nu_e, \bar{\nu}_e$ (Popham, Woosley & Fryer 1999). The flux density of ν_x rapidly increases near the inner boundary and reaches to be comparable with $F_{\bar{\nu}_e}$. The profile of the total flux density is expressed approximately as $F(r) = F_{\nu_e} + F_{\bar{\nu}_e} + F_{\nu_x} \approx 3.8 \times 10^{40} r_*^{-2.9}(\mathrm{erg/cm}^2/\mathrm{sec})$.

4.4 Luminosity and mean energy of neutrinos

The angular momentum of a black hole changes the efficiency of viscous heating through the shear stress $\sigma_{r\varphi}$. The energy equation

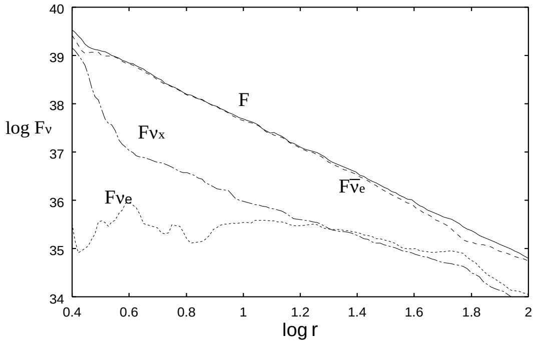

Figure 13. The profiles of total flux density of neutrinos F, flux density of antielectron neutrinos $F_{\bar{\nu}_e}$, that of heavy neutrinos F_{ν_x}, and that of electron neutrinos F_{ν_e}. The unit of flux density F is (erg cm^{-2}sec^{-1}). The parameters of accretion are same as in Fig. 11.

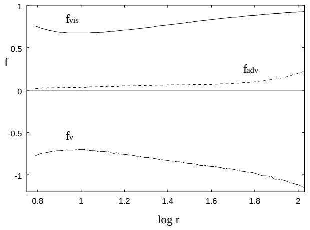

Figure 14. The profiles of relative rates of heating and cooling. The relative heating rates due to viscosity f_{vis}, due to compression f_{adv}, and the relative cooling rate due to neutrino loss f_ν are plotted in the case with $a = 0, M_{BH} = 3\mathrm{M}_\odot, \dot{M} = 0.1\mathrm{M}_\odot$ sec^{-1}.

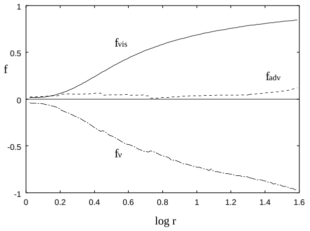

Figure 15. The same as Fig.14, but for the case of a rapidly rotating black hole with $a = 1$, $M_{BH} = 3\mathrm{M}_\odot$ are depicted, where $\dot{M} = 0.02\mathrm{M}_\odot$ sec^{-1}.

is expressed such as

$$\begin{aligned}\frac{\partial E}{\partial t} &= Q^+ - Q^- \\ &= 0.98\times 10^{43}(\mathrm{erg/sec/cm^2})\dot{m}m^{-2}r_*^{-3}(f_{vis}+f_{adv}+f_\nu) \\ &= 0, \end{aligned} \tag{58}$$

where f_{vis}, f_{adv} and f_ν are the factors of energy flux by viscous heating, by advectional heating and by neutrino cooling. These factors, f_{vis}, f_{adv}, f_ν, for $a = 0$ and 1 are shown in Fig. 14 and 15. The absolute values of f_{vis} and f_ν are orders of unity except for the inner side of the disk with $a = 1$. In the case of extreme Kerr, $a = 1$, the efficiency of viscous heating f_{vis} decreases to be $f_{vis} \approx 0.05$ at the inner boundary of the disk. The factor of advection, f_{adv}, is relatively small and positive, $f_{adv} \approx 0.05$. The accretion with the Keplerian angular momentum heats up the flow by the compression. On the other hand the advection dominant accreting flow(ADAF) cools the flow by the extension of the fluid (Di Matteo, Perna, & Narayan 2002; Narayan, Piran, & Kumar 2001; Popham, Woosley & Fryer 1999).

If the luminosity of each flavor of neutrino and its mean energy are observed (Halzen & Hooper 2002; McDonald A.B. et al. 2003; McKinsey & Coakley 2004), the physical structure around a black hole will be made clear. Though the electron neutrinos, ν_e, are somewhat absorbed in the accreting matter at the outside of the disk, the antielectron neutrinos, $\bar{\nu}_e$, and heavy neutrinos, ν_x, are little absorbed there. The energy flux of ν_e at the surface is very small in comparison with those of other types of neutrinos. Thus we calculate the luminosity L_{ν_i} and the mean energy $\bar{E}_{\nu_i}$ for each type of neutrino ν_i emitted from the surface of the disk, and then discuss the effects of the absorption of ν_e at the outer atmosphere of the disk if necessary. The luminosity measured at infinity is expressed in the Boyer-Lindquist coordinate as $L_{\nu_i} = \int q^z_{\nu_i}(r)dS_z$, where $q^z_{\nu_i}(r)$ is the z component of the flux density vector at the radius r, and dS_z is the z component of the surface element vector. The component $q^z_{\nu_i}$ is connected with the local surface density F_{ν_i} such as $q^z_{\nu_i} = e^{\hat{t}}_t F_{\nu_i}$, where $e^{\hat{t}}_t$ is the t component of the orbiting basis $\vec{\omega}^{\hat{t}}$ (23). Thus the luminosity is expressed by

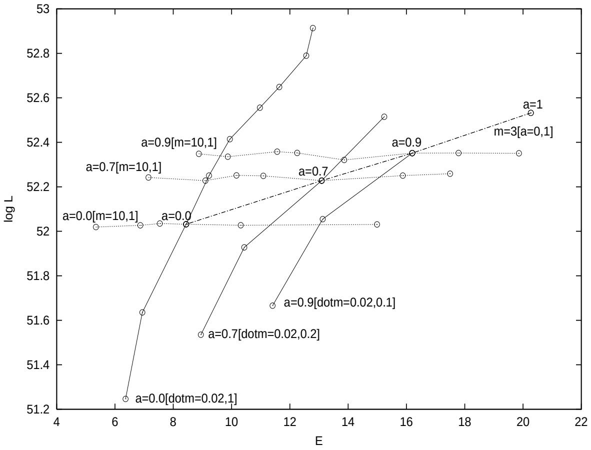

Figure 16. The neutrino luminosity L(erg/sec) versus mean energy of ejected neutrinos E(MeV) observed at infinity. The luminosity L and mean energy E for the variation of specific angular momentum of a black hole, $a = 0 \rightarrow 1$, are depicted by the dot-dashed line labeled as $m = 3[a = 0, 1]$, where the other parameters of accretion are fixed to be $M_{BH} = 3\mathrm{M}_\odot, \dot{M} = 0.1\mathrm{M}_\odot$/sec. Those for $M_{BH} = 1, 2, 3, 4, 5, 6, 8, 10(\mathrm{M}_\odot)$ are connected by the line labeled as $a = 0.9[m = 10, 1]$, where $a = 0.9, \dot{M} = 0.1\mathrm{M}_\odot$/sec. Those for $\dot{M} = 0.02, 0.05, 0.1(\dot{M}_\odot$ sec^{-1}) are labeled as $a = 0.9[dotm = 0.02, 0.1]$, where $a = 0.9, M_{BH} = 3\mathrm{M}_\odot$. Those for $a = 0, 0.7$ are similarly shown.

$$L_{\nu_i} = 2\pi\int_{r_h}^{\infty}\gamma(1+v_\omega v_{(\varphi)})F_{\nu_i}rdr. \tag{59}$$

The mean energy $\bar{E}_{\nu_i}$ is defined as follows. When the neutrinos are thermally equilibrium in the matter, the local mean energy of neutrinos $\bar{\epsilon}_{\nu_i}(r)$ is expressed by the matter temperature $T(r)$ and the degeneracy factor of neutrino $\eta_{\nu_i}(r)$, $\bar{\epsilon}_{\nu_i}(r) = kT(r)F_3(\eta_{\nu_i}(r))/F_2(\eta_{\nu_i}(r))$, where $F_k(\eta_{\nu_i})$ is the Fermi integral $F_k(\eta) \equiv \int_0^\infty(1+\exp{(x-\eta)})^{-1}x^k dx$. The number per unit time emitted from the differential ring over the width of radius $r \sim r+dr$ is $dN_{\nu_i}(r) = dF_{\nu_i}(r)/\bar{\epsilon}_{\nu_i}(r)$, where $dF_{\nu_i}(r)$ is the energy flux of neutrino from the ring. The total number of neutrino is $N_{\nu_i} = \int_{r_h}^\infty dN_{\nu_i}(r)$. Thus the mean energy is defined by $\bar{E}_{\nu_i} = L_{\nu_i}/N_{\nu_i}$.

The total luminosity for all types of neutrinos is $L_\nu = \sum_i L_{\nu_i}$. The mean energy in all types of neutrinos is simply defined by $\bar{E}_\nu = L_\nu/\sum_i N_{\nu_i}$. We set the quantities of neutrinos within r_{ms} to be same as the values at the boundary $r = r_{ms}$. The maximum radius of the integral is taken to be $r_{max} = 10^2 r_{ms}$.

The total luminosities and the mean energies measured at infinity, L_ν, $\bar{E}_\nu$, are plotted in Fig. 16 for some typical black holes with $m = 1 \sim 10$ and $a = 0 \sim 1$ and for the accretion rate $\dot{m} = 0.02 \sim 1$. The rotating black hole has a small radius of the inner boundary, r_{ms}, where the high density of accreting matter increases the emissivity of neutrinos, which brings about the large luminosity L_ν with high mean energy $\bar{E}_\nu$. It is superior to the inefficiency of viscosity even if $a \to 1$ and $f_{vis} \to 0.05$. When the mass of a black hole is $M_{BH} = 3\mathrm{M}_\odot$ and the accretion rate is $\dot{M} = 0.1\mathrm{M}_\odot$/sec, the ratio of luminosity is $L_\nu(a = 1)/L_\nu(a = 0) \approx 3.5$, and that of mean energy is $\bar{E}_\nu(a = 1)/\bar{E}_\nu(a = 0) \approx 2.5$. The luminosity is proportional to the accretion rate, $L_\nu \propto \dot{M}$, but is independent of the mass scale of a black hole, M_{BH}, that is, the constant ratio of the gravitational binding energy of accreting matter is released into the neutrino's energy through the viscous heating. Its ratio increases according to a. The mean energy $\bar{E}_\nu$ is proportional to $\dot{M}$ but is inversely proportional to M_{BH}, $\bar{E}_\nu \propto \dot{M}^{0.8} M_{BH}^{-1.07}$. When each type of neutrino ejected from a GRB is observed, the physics around a black hole will be made more clear. The observed luminosities of neutrinos and their mean energies will determine the physical parameters of a central black hole, a, M_{BH}, and the accretion rate, $\dot{M}$, from the diagram shown in Fig. 16.

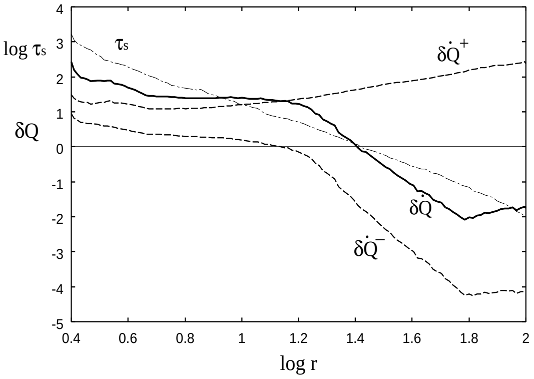

Figure 17. The variation of net heating rate $\delta\dot{Q}$ due to the increase of temperature δT within the diffusion time. The variation of the rate by the viscous and compressing heating $\delta\dot{Q}^{+}$, and that by the neutrino cooling $\delta\dot{Q}^{-}$ are plotted by dashed lines. The scattering optical depth of antielectron neutrinos τ_s is plotted by dot-dashed line. The parameters of accretion are $\dot{M} = 0.5\mathrm{M}_\odot\mathrm{sec}^{-1}, M_{BH} = 3\mathrm{M}_\odot, a = 0.9, \alpha_{vis} = 0.1$.

5 DISCUSSION

We have studied the accretion in simplified model in which the disk is assumed to be stationary and its vertical structure is treated by one-zone model with the thickness, H. These simplifications might restrict the properties of the accretion disk. We first discuss the thermal stability of the disk. In the stationary state, the cooling rate due to neutrino's loss must be equal to the production rate of thermal energy in the disk even if neutrinos are scattered in many times within the disk. The accretion disk is thermally stable since the antielectron neutrinos $\bar{\nu}_e$ are little absorbed in the disk and can sufficiently carry out the perturbed thermal energy. However in the short duration within the diffusion time, $t_{diff} \approx \tau_s H/c \approx 10$(ms), the perturbed energy is stayed in the disk. The heating or cooling time then becomes $t_{heat} = t_{cool} =\approx \epsilon/q \approx$a few ms, i.e., $t_{heat} < t_{diff}$. If the accretion disk is thermally unstable, the perturbations rapidly grow. This stability should be decided by the fully nonstationary treatment of accretion disk. Here we discuss it in brief by the perturbation analysis. When the scattering optical depth is large $\tau_s \gg 1$ and the absorbing optical depth is negligible, $\tau_a \ll 1$, the neutrinos stay in the disk in τ_s times of the crossing time $t_{cross} = H/c$. When $\tau_s \ll 1$, the perturbation of the cooling rate is expressed as $\delta Q^- = \delta F_\nu = \delta(q_\nu H)$. We provide the perturbation of the cooling rate in the thick case as $\delta Q^- = \delta(q_\nu H/\tau_s)$. The perturbed cooling rates by $\bar{\nu}_e$ and ν_x are then set to be $\delta Q^-_{\bar{\nu}_e} + \delta Q^-_{\nu_x} = \delta(q_{\bar{\nu}_e} H/(1 + \tau_s(\bar{\nu}_e))) + \delta(q_{\nu_x} H/(1 + \tau_s(\nu_x)))$. Since the electric neutrinos ν_e are almost absorbed, the perturbed cooling rate is expressed as $\delta Q^-_{\nu_e} = \delta(q_{\nu_e} H/(1.5\tau_{\nu_e a}\tau_{\nu_e} + \sqrt{3}\tau_{\nu_e a} + 1))$.

The perturbation of the heating rate is brought about by the viscous heating and the compression, $\delta Q^+ = \delta Q_{vis} + \delta Q_{adv}$. We thus evaluate the thermal stability for the perturbation of temperature δT with the restriction of constant surface density Σ,

$$\delta Q = \left(\frac{\partial \log Q^+}{\partial \log T}\right)_\Sigma + \left(\frac{\partial \log Q^-}{\partial \log T}\right)_\Sigma. \tag{60}$$

The results for δQ are shown in Fig. 17, where $\dot{m} = 0.5, m = 3, a = 0.9 and \alpha_{vis} = 0.1$. The sign of δQ becomes positive when $\tau_s(\bar{\nu}_e) \geqslant 1$. The sign of $\delta Q^- = (\partial \log Q^-/\partial \log T)_\Sigma$ also becomes positive when $\tau_s(\bar{\nu}_e) \geqslant 10$, since the opacity of $\bar{\nu}_e$ increases according to the rise in temperature, $\delta T > 0$. For the region where the scattering optical depth of $\bar{\nu}_e$ is larger than unity, $\tau_s(\bar{\nu}_e) \geqslant 1$, the accretion disk becomes thermally unstable at least within the duration of the diffusion time.

We next discuss the interaction between neutrinos and nucleons. The spectrums of neutrino are assumed here to be Ferm-Dirac distributions with local temperature being equal to that of nucleon medium. In the neutrino sphere(disk) the neutrinos are thermally equilibrium with nucleons but in the outer layer above it the above assumption is in general not consistent. In the outer layer the spectral temperature defined by the mean energy of neutrinos, $T_* \equiv \bar{E}_\nu/3$, becomes higher than the nucleon's temperature (Raffelt 2001). Since the mean energy of neutrino exceeds the rest mass energy of electron, $\bar{E}_\nu > m_e c^2$, the collision between neutrinos and electrons effectively transfer the momentum and energy from neutrinos to electrons (Thompson, Burrows, & Horvath 2000). The dynamic structure functions which include the full kinematics of ν_i-nucleon scattering produce also the tranfers of energy and momentum between neutrinos ν_i and nucleons. In the diffusion zone in which the neutrinos many scatter the electrons and nucleons, $\tau_s \geqslant 1$, the convection originated by neutrinos may work important effects on the dynamics of the medium. In our accretion model the effective optical depth, $\tau_{eff} \equiv \sqrt{\tau_a \tau_s}$, exceeds unity only for ν_e. The thermal equilibrium disk of ν_e is formed at $r \approx 10 r_g$. The scattering optical depths of all flavors, $\tau_s(\nu_e), \tau_s(\bar{\nu}_e), \tau_s(\nu_x)$, exceed unity. In the diffusion zone above the disk, $z \geqslant H$, the neutrinos might push the nucleon matter outward and might drive the convection or wind or jets.

Our results for the hot, dense matter accretion onto a black hole indicate that the emissivity of electron antineutrinos $q_{\bar{\nu}_e}$ is very efficient and the fraction of free protons is extremely minute, which allows the accretion disk effectively cooled by $\bar{\nu}_e$. On the other hand the electron neutrinos ν_e are almost trapped by many free neutrons. The accretion disk cooled by neutrinos could be thermally unstable at least within the diffusion time, $t_{diff} \approx 10$(ms). Our treatment of the accretion is very simple, stationary model with the homogeneous disk in the vertical direction. The compactness problem for GRBs requires the formation of relativistic jets. The accretion should be further solved in unstationary, 2- or 3- dimensional treatment with the transfers of neutrinos.

ACKNOWLEDGMENTS

I thank Professor T. Yoshida for helpful discussions, Professor S. Yanagita for some helpful suggestions and an anonymous referee for very useful comments that improved the presentation of the paper.

REFERENCES

Abramowicz M., Jaroszyński, Sikora M., 1978, A&A, 63, 221
Bardeen J. M., Press W. H., Teukolsky S. A., 1972, ApJ, 178, 347
Bruenn S.W. 1985, ApJS, 58, 771
Burbidge E.M., Burbidge G.R., Fowler W.A., Hoyle, F., 1957, Rev. Mod. Phys. 29, 547
Burrows A., 2001, PPNPHYSP, 46, 59
Carigan B.J., Katz J.I., 1992, ApJ, 399, 100
J. Cooperstein., Van Den Horn L.J., Baron, E.A., 1986, ApJ, 309, 653
Cooperstein J., Van Den Horn L.J., Baron, E.A., 1986, ApJ, 315, 729
Di Matteo T., Perna R., Narayan R., 2002, ApJ, 579, 706
Ferdinado P., et al., 2001, ApJ, 555, 900
Greiner J. 2004, http://www.mpe.mpg.de$\sim$jcg/grbrsh.html
Guibert P.W., Fabian A.C., Rees, M., 1983, MNRAS, 205, 593
Halzen F., Hooper D., 2002 astro-ph/0204527
Hubeny I., 1990, ApJ, 351, 632
Kawabata K. S., et al. 2003, ApJ, 593, L19
Kohri K., Mineshige S. 2002, ApJ, 577, 311
Lipkin Y. M., et al., 2004, astro-ph/0312594
Lloyd-Ronning N.M., and Ramirez-Ruiz, E., 2002, ApJ, 576, 101
Lyutikov M., Blandford R.D., 2003, astro-ph/0312347
Landau L.D., Lifshitz E.M., 1964, in vol 5 of Cource of Theoretical Physics (Pergamon Press, Oxford)
Lattimer J.M., Swesty F. D., 1992, NPGYSA, 535, 331
Matheson T., et al., 2003, ApJ, 599, 394
MacFadyen A.I., Woosley S.E., 1999, ApJ, 524, 262
McDonald A.B., Spiering C., Sch$\ddot{o}$nert S., Kearns, E.T., Kajita T., 2003, astro-ph/0311343
McKinsey D.N., Coakley K.J., 2004, astro-ph/0402007
Meyer B.S., Mathews G.J., Howard W.M., Woosley S.E., Hoffman R.D., 1992, ApJ, 399, 656
Misner C.W., Thorne K.S., Wheeler J.A., 1973, Gravitation (Freeman, San Francisco)
Narayan R., Piran T., Kumar, P., 2001, ApJ, 557, 949
Novikov I., Thorne K.S., 1973, in Black Holes, eds. B. DeWitt and C. DeWitt, Gordon and Breach, New York
Piran T., 1999, PHYSREP, 314, 575
Popham R., Narayan R., 1995, ApJ, 442, 337
Popham R., Woosley S.E., Fryer, C., 1999, ApJ, 518, 356
Qian Y.Z., Woosley S.E., 1996, ApJ, 471, 331
Raffelt G.G., 2001, ApJ, 561, 890
Ruffert M., Janka H.-Th., Schafer G., 1996, A&A, 311, 532
Schinder P.J., Schramm D.N., Margolis S.H., Tubbs D.L., 1987, ApJ, 313, 531
Shapiro S.L., Teukolsky S.A., 1983, in Black Holes, White Dwarfs and Neutron Stars (John Wiley & Sons, New York and Chichester)
Stathakis R. A., et al., 2000, MNRAS, 314, 807
Stern B.E., Tikhomirova Y., Kompaneets D., Svensson R., and Poutanen J., 2001, ApJ, 563, 80
Thompson T.A., Burrows A., Horvath, J.E., 2000, PhRvC, 62c, 035802
Thompson T. A., Chang, P., Quataert, E., 2004, astro-ph/0401555
Thorne K. S., Price R. H., Macdonald, D. A., 1986, in Black Holes The Membrane Paradigm(New Haven: Yale Univ. Press)
Tubbs D.L., Schramm D.N., 1975, ApJ, 201, 467
Turner N.J., 2004, ApJ, 605, L45
Usov V. V., 1992, Nature, 357, 472
Vanderspek R., et al., 2004, astro-ph/0401311
Woosley S. E., 1993, ApJ, 405, 273
Yokosawa M., 1995, PASJ, 47, 605

APPENDIX A: REACTION RATES OF NEUTRINOS

The neutrino cross sections, opacities, emissivities and reaction rates used in our model are listed in Table A1–4. The numerical functions used in the reaction rates are listed in Table A5.

APPENDIX B: TRANSFERS OF NEUTRINOS IN A PLANE-PARALLEL DISK

The analytic formulas of neutrino's transfers are derived by using the simplified treatment of radiative transfer given by Popham, & Narayan (1995). Introducing the two streams, with intensities I^+, I^- moving at an angle $\cos\theta = 1/\sqrt{3}$ relative to $+z$ and $-z$, define the net flux density j and the total intensity $\bar{j}$ such as $j = (I^+ - I^-)/2\sqrt{3}$ and $\bar{j} = (I^+ + I^-)/2$ (Popham, & Narayan 1995). The transfers of neutrinos are then described by the production rate of neutrinos, $\dot{n}^+$, and the absorption opacity, scattering opacity and the total opacity, κ_a, κ_s and $\kappa = \kappa_a + \kappa_s$, as

$$\frac{dj}{dz} = -\kappa_a \bar{j} + \dot{n}^+ \tag{B1}$$

$$\frac{d\bar{j}}{dz} = -3\kappa j. \tag{B2}$$

The boundary condition at the center of the disk is $j = 0$. To derive the simplest solution, let us assume that $(\dot{n}^+ - \kappa_a \bar{j}), \kappa$ are independent of z (Hubeny 1990). Equations (B1) and (B2) can then be integrated to give

$$j(z) = (\dot{n}^+_c - \kappa_a \bar{j}_c) z \tag{B3}$$

$$\bar{j}(z) = \bar{j}_c - \frac{3}{2}\kappa(\dot{n}^+_c - \kappa_a \bar{j}_c) z^2, \tag{B4}$$

where $\dot{n}^+_c$ and $\bar{j}_c$ are the values of $\dot{n}^+$ and $\bar{j}$ at $z = 0$. The boundary condition at the surface of the disk is $j^- = 0$, i.e., $\bar{j} = \sqrt{3} j$. Applying this boundary condition we find

$$\bar{j}_c = \frac{\sqrt{3} + 1.5\tau}{1 + \sqrt{3}\tau_a + 1.5\tau\tau_a} \dot{n}^+_c H, \tag{B5}$$

where τ_a is the absorbing optical depth, $\tau_a = \kappa_a H$, and τ is the total optical depth, $\tau = \kappa H$. The escaping flux density of any sort of neutrino, ν_i, is then given by

$$F_{n(\nu_i)} = j(H) = \frac{\dot{n}^+_{\nu_i} H}{1.5\tau_{\nu_i a}\tau_{\nu_i} + \sqrt{3}\tau_{\nu_i a} + 1}, \tag{B6}$$

where τ_{ν_i} and $\tau_{\nu_i a}$ are the total optical depth and the absorbing one of ν_i, and $\dot{n}^+_{\nu_i}$ is the production rate of ν_i per unit volume.

Table A1. Cross section

No.	Neutrino Reaction	Cross Section	
1	$\nu_e + n \rightarrow e + p$	$\sigma^a_{\nu_e,n}(\varepsilon_{\nu_e}) = \sigma_0(1+3g_A^2)\left(\frac{\varepsilon_{\nu_e}+Q}{2m_ec^2}\right)^2[1-\left(\frac{m_ec^2}{\varepsilon_{\nu_e}+Q}\right)^2]^{1/2}W_M$	
2	$\bar{\nu}_e + p \rightarrow e^+ + n$	$\sigma^a_{\bar{\nu}_e,p}(\varepsilon_{\bar{\nu}_e}) = \sigma_0(1+3g_A^2)\left(\frac{\varepsilon_{\bar{\nu}_e}-Q}{2m_ec^2}\right)^2[1-\left(\frac{m_ec^2}{\varepsilon_{\bar{\nu}_e}-Q}\right)^2]^{1/2}W_{\bar{M}}$	
3	$\nu_i + p \rightarrow \nu_i + p$	$\sigma^s_p(\varepsilon_{\nu_i}) = \sigma_0\left(\frac{\varepsilon_{\nu_i}}{2m_ec^2}\right)^2[4\sin^4\theta_W - 2\sin^2\theta_W + \frac{1+3g_A^2)}{4}]$	[a]
p 4	$\nu_i + n \rightarrow \nu_i + n$	$\sigma^s_n(\varepsilon_{\nu_i}) = \sigma_0\left(\frac{\varepsilon_{\nu_i}}{2m_ec^2}\right)^2\left(\frac{1+3g_A^2)}{4}\right)$	
5	$\nu_i + e \rightarrow \nu_i + e$	$\sigma_e = \sigma_0\frac{1}{8}\left[(C_V+C_A)^2 + \frac{1}{3}(C_V-C_A)^2\right]\left(\frac{\varepsilon_{\nu_i}}{m_ec^2}+\frac{1}{2}\right)$	

[a] These cross sections are given by Burrows(2001). A convenient reference neutrino cross section is $\sigma_0 = \frac{4G_F^2(m_ec^2)^2}{\pi(hc/2\pi)^4} \simeq 1.705 \times 10^{-44}\mathrm{cm}^2$. g_A is the axial-vector coupling constant (~ -1.26), θ_W is the Weinberg angle and $\sin^2\theta_W \simeq 0.23$, $Q = m_nc^2 - m_pc^2 = 1.29332\mathrm{MeV}$, and for a collision in which the electron gets all of the kinetic energy $\varepsilon_{e^-} = \varepsilon_{\nu_e} + Q$. W_M is the weak magnetism/recoil correction and is approximately equal to $(1 + 1.1\varepsilon_{\nu_e}/m_nc^2)$. $C_V = 1/2 + 2\sin^2\theta_W$ for ν_e and $\bar{\nu}_e$ neutrinos, $C_V = -1/2 + 2\sin^2\theta_W$ for ν_x and $\bar{\nu}_x$ neutrinos, $C_A = +1/2$ for $\nu_e, \bar{\nu}_\mu$ and $\bar{\nu}_\tau$ neutrinos, and $C_A = -1/2$ for $\bar{\nu}_e, \nu_\mu$ and ν_τ neutrinos.

Table A2. Opacity

No.	Neutrino Reaction	Opacity	References	
1	$\nu_e + n \rightarrow e + p$	$\kappa^a_\beta = \eta_{np}\frac{\int d^3pf_{\nu_e}(\varepsilon)\sigma^a_{\nu_e,n}(\varepsilon)[1-f_e(\varepsilon_{\nu_e}+Q)]}{\int d^3pf_{\nu_e}(\varepsilon)}$	Burrows(2001)	
		$\approx 4.3\times10^{-6}(\mathrm{cm}^{-1})\rho_{12}Y_{np}T_{11}^2\frac{F_4^+(\eta_{\nu_e},\eta_e,q)}{F_2(\eta_{\nu_e})}$		
2	$\bar{\nu}_e + p \rightarrow e^+ + n$	$\kappa^a_{\bar{\beta}} \approx 4.3\times10^{-6}(\mathrm{cm}^{-1})\rho_{12}Y_{pn}T_{11}^2\frac{F_4^+(\eta_{\bar{\nu}_e},\eta_{e^+},-q)}{F_2(\eta_{\bar{\nu}_e})}$	Burrows(2001)	
3	$\nu_i + \bar{\nu}_i + N + N \rightarrow N + N$	$\kappa^a_{NN} \approx \frac{3C_A^2G_F^2n_BT^5\Gamma}{\pi^2}\frac{2}{5\varepsilon_\nu}$	Raffelt(2001)	
		$\approx 1.43\times10^{-9}(\mathrm{cm}^{-1})(X_n\rho_{12})^2T_{11}^2\frac{F_2(\eta_{\nu_i})}{F_3(\eta_{\nu_i})}\left(\frac{3}{2+0.862T_{11}}\right)^{1/2}$		
4	$\nu_e + A \rightarrow e + A'$	$\kappa^a_A = \frac{\alpha^2}{4}\sigma_0n_Ae^{\eta_n-\eta_p-q'}\frac{2}{7}N_p(Z)N_h(N)$		[a].
		$\left(\frac{kT}{m_ec^2}\right)^2\frac{F_4^{q'-}(\eta_{\nu_e},\eta_e)}{F_2(\eta_{\nu_e})}$	Bruenn(1985)	
		$\approx 1.2\times10^{-6}(\mathrm{cm}^{-1})\rho_{12}Y_AT_{11}^2f_A(\eta)$		
5	$\nu_i + N \rightarrow \nu_i + N$	$\kappa^s_N \approx 1.1\times10^{-6}(\mathrm{cm}^{-1})\rho_{12}T_{11}^2C_{s,N}Y_{NN}\frac{F_4(\eta_{\nu_i})}{F_2(\eta_{\nu_i})}$	Burrows(2001)	
t 6	$\nu_i + e \rightarrow \nu_i + e$	$\kappa^s_e \approx 1.66\times10^{-6}(\mathrm{cm}^{-1})Y_e\rho_{12}T_{11}^2\frac{F_4(\eta_{\nu_i})}{F_2(\eta_{\nu_i})}$	Burrows(2001)	
7	$\nu_i + A \rightarrow \nu_i + A$	$\kappa^s_A = \frac{a_0^2}{6}\sigma_0n_AA^2\left(\frac{kT}{m_ec^2}\right)^2\frac{F_4(\eta_{\nu_i})}{F_2(\eta_{\nu_i})}$	Bruenn(1985)	
		$\approx 2.3\times10^{-7}(\mathrm{cm}^{-1})\rho_{12}T_{11}^2A^2Y_A\frac{F_4(\eta_{\nu_i})}{F_2(\eta_{\nu_i})}$		

[a] The absorption opacity κ_a and scattering opacity κ_s are expressed with unit cm^{-1}. $F_k(\eta)$ is the Fermi integral $F_k(\eta) \equiv \int_0^\infty \frac{x^kdx}{1+\exp(x-\eta)}$. The complex integrals, $F_4^+(\eta_{\nu_e},\eta_e,q)$ and $F_4^{q'-}(\eta_{\nu_e},\eta_e)$, are shown in Table A5. The doubly indexed quantity Y_{np} is the number fraction defined as $Y_{np} = \eta_{np}/n_B$, and Y_{pn} is $Y_{pn} = \exp(\eta_p - \eta_n)Y_{np}$, where η_{np} is the dynamic structure factor for neutrino-neucleon interaction, $\eta_{np} = \int\frac{2d^3p}{(2\pi)^3}f_n(\varepsilon)[1-f_p(\varepsilon)] = \frac{n_p-n_n}{\exp(\eta_p-\eta_n)-1}$. Y_{NN} is $Y_{NN} = \frac{Y_N}{1+\frac{2}{3}\max(\eta_N,0)}$, and $C_{s,N}$ is $C_{s,N} = 1$ if $N = n$ and $C_{s,N} = 0.827$ if $N = p$. A is the mean mass number of heavy nuclei, n_A is the number density of heavy nuclei and Y_A is the fraction, $Y_A = n_A/n_B$. X_n is the mass fraction of neutrons. $f_A(\eta)$ is $f_A(\eta) = e^{\eta_n-\eta_p-q'}\frac{2}{7}N_p(Z)N_h(N)\frac{F_4^{q'+}(\eta_{\nu_e},\eta_e)}{F_2(\eta_{\nu_e})}$, where $q' \approx \eta_n - \eta_p + \Delta$, $\Delta = \frac{3\mathrm{MeV}}{kT}$. $N_p(Z)$ and $N_h(N)$ are $N_p(Z) = \{0 \text{ for } Z < 20;\ Z - 20 \text{ for } 20 < Z < 28;\ 8 \text{ for } Z > 28\}$, and $N_h(N) = \{6 \text{ for } N < 34;\ 40 - N \text{ for } 34 < N < 40;\ 0 \text{ for } N > 40\}$. The density ρ_{12} and temperature T_{11} are normalized vales by 10^{12}(g/cm^3) and 10^{11}K

APPENDIX C: CHANGING RATES OF POSITRONS ALONG THE FLOW

The number density of positrons which are equilibrium with thermal photons is described as

$$n_{e^+th} = \frac{1.8}{\pi^2}\left(\frac{kT}{hc/2\pi}\right)^3 < 1 - f(\eta_e) >< 1 - f(\eta_{e^+}) > . \quad \text{(C1)}$$

(Landau and Lifshitz 1964), where the brackets indicate the mean values of the phase space blocking factors. These factors are eval-

Table A3. Emissivity

No.	Neutrino Reaction	Emission Rate	References
1	$e + p \rightarrow \nu_e + n$	$q_\beta(\nu_e) = \eta_{pn} \frac{4\pi c}{(hc)^3} \int_0^\infty d^3p\varepsilon f_e(\varepsilon + Q)\sigma^a_{\nu_e,n}(\varepsilon)[1 - f_{\nu_e}(\varepsilon)]$	Burrows(2001)
		$\approx 7.4 \times 10^{33}(\mathrm{ergcm}^{-3}\mathrm{sec}^{-1})\rho_{12}T^6_{11}Y_{pn}F^-_5(\eta_{\nu_e}, \eta_e, q)$	
2	$e^+ + n \rightarrow \bar{\nu}_e + p$	$q_{\bar{\beta}}(\bar{\nu}_e) \approx 7.4 \times 10^{33}(\mathrm{ergcm}^{-3}\mathrm{sec}^{-1})\rho_{12}T^6_{11}Y_{np}F^-_{5+}(\eta_{\bar{\nu}_e}, \eta_{e^+}, q)$	Burrows(2001)
3	$N + N \rightarrow N + N + \nu_i + \bar{\nu}_i$	$q_{NN}(\nu_i, \bar{\nu}_i) \approx 7.3 \times 10^{30}(\mathrm{ergcm}^{-3}\mathrm{sec}^{-1})(X_N\rho_{12})^2T^{5.5}_{11}$	Burrows(2001)
4	$e + A \rightarrow \nu_e + A'$	$q_A(\nu_e) = b\sigma_0\frac{\alpha^2}{4}N_A\frac{2}{7}N_p(Z)N_h(N)\left(\frac{kT}{m_ec^2}\right)^5 kTF^{q'-}_5(\eta_{\nu_e}, \eta_e)$	Bruenn(1985)
		$\approx 2.06 \times 10^{33}(\mathrm{ergcm}^{-3}\mathrm{sec}^{-1})\rho_{12}Y_A\frac{2}{7}N_p(Z)N_h(N)T^6_{11}F^{q'-}_5(\eta_{\nu_e}, \eta_e)$	
5	$n + n \rightarrow n + p + e + \nu_e$	$q_{URCA}(\nu_e) = 2.7 \times 10^{34}(\mathrm{ergcm}^{-3}\mathrm{sec}^{-1})\rho^{2/3}_{12}T^8_{11}F_Q(\eta_e, \eta_{\nu_e})$	Shapiro et al.(1983)
6	$\gamma \rightarrow \nu_i + \bar{\nu}_i$	$q_\gamma(\nu_e, \bar{\nu}_e) \approx 1.20 \times 10^{33}(\mathrm{ergcm}^{-3}\mathrm{sec}^{-1})T^9F_{Q\gamma}(\eta_{\nu_e})$	Ruffert et al.(1996)
		$q_\gamma(\nu_x) \approx 8.3 \times 10^{30}(\mathrm{ergcm}^{-3}\mathrm{sec}^{-1})T^9F_{Q\gamma}(\eta_{\nu_x})$	Ruffert et al.(1996)
7	$e + e^+ \rightarrow \nu_i + \bar{\nu}_i$	$q_{ee}(\nu_e, \bar{\nu}_e) \approx 1.24 \times 10^{33}(\mathrm{ergcm}^{-3}\mathrm{sec}^{-1})T^9_{11}f_{\nu_e}(\eta)$	Thompson et al.(2000)
		$q_{ee}(\nu_x, \bar{\nu}_x) \approx 5.49 \times 10^{32}(\mathrm{ergcm}^{-3}\mathrm{sec}^{-1})T^9_{11}f_{\nu_x}(\eta)$	Thompson et al.(2000)

[a].

[a] The emission rates q are expressed with unit erg/cm^3/sec. The complex integrals, $F^-_5(\eta_{\nu_e}, \eta_e, q), F^-_{5+}(\eta_{\bar{\nu}_e}, \eta_{e^+}, q)$ and $F^{q'}_5(\eta_{\nu_e})$, are shown in Table A5. F_Q and f_{ν_i} for $i = e, x$ are $F_Q(\eta_e, \eta_{\nu_e}) =< 1 - f_e(\varepsilon_e) >< 1 - f_{\nu_e}(\varepsilon_{\nu_e}) >$ and $f_{\nu_i}(\eta) = \frac{F_4(\eta_e)F_3(\eta_{e^+})+F_4(\eta_{e^+})F_3(\eta_e)}{2F_4(0)F_3(0)} < 1 - f_{\nu_i}(\varepsilon) >_{ee}< 1 - f_{\bar{\nu}_i} >_{ee}$. $F_{Q\gamma}(\eta_{\nu_e})$ is $F_{Q\gamma}(\eta_{\nu_e}) = \gamma^6e^{-\gamma}\frac{1}{2}((1+(\gamma+1)^2) < 1 - f_{\nu_e}(\varepsilon) >_\gamma< 1 - f_{\bar{\nu}_e}(\varepsilon) >_\gamma$, where γ and γ_0 are $\gamma \approx \gamma_0\sqrt{\pi^2/3 + \eta^2_e}$, $\gamma_0 = h\Omega_0/(2\pi m_ec^2) = 5.565 \times 10^{-2}$. The mean blocking factors $< 1 - f_{\nu_i}(\varepsilon) >_{ee}$, .. are described in Table A5. The density ρ_{12} and temperature T_{11} are normalized vales by 10^{12}(g/cm^3) and 10^{11}K

Table A4. Fraction Change

No.	Neutrino Reaction	Fraction Change
1	$\nu_e + n \rightleftharpoons e + p$	$\dot{Y}_e(\beta) = \frac{4\pi c}{(hc)^3}\int_0^\infty d^3p\sigma^a_{\nu_e,n}(\varepsilon)\Big[Y_{np}f_{\nu_e}(\varepsilon)[1 - f_e(\varepsilon + Q)] - Y_{pn}f_e(\varepsilon + Q)[1 - f_{\nu_e}(\varepsilon)]\Big]$
		$\approx 9.0 \times 10^2(\mathrm{sec}^{-1})T_{11}[Y_{np}F^+_4(\eta_{\nu_e}, \eta_e, q) - Y_{pn}F^-_4(\eta_{\nu_e}, \eta_e, q)]$
2	$\nu_e + A \rightleftharpoons e + A'$	$\dot{Y}_e(A) = b\frac{\alpha^2}{4}\sigma_0Y_A\frac{2}{7}N_p(Z)N_h(N)\left(\frac{kT}{m_ec^2}\right)^5\left(e^{\eta_n-\eta_p-q'}F^{q'+}_4(\eta_{\nu_e}, \eta_e) - F^{q'-}_4(\eta_{\nu_e}, \eta_e)\right)$
		$\approx 2.4 \times 10^2(\mathrm{sec}^{-1})T^5_{11}Y_A\frac{2}{7}N_p(Z)N_h(N)\left(e^{\eta_n-\eta_p-q'}F^{q'+}_4(\eta_{\nu_e}, \eta_e) - F^{q'-}_4(\eta_{\nu_e}, \eta_e)\right)$
3	$n + n \rightarrow n + p + e + \nu_e$	$\dot{Y}_e(URCA) \approx \frac{q_{URCA}}{\bar{\varepsilon}_{\nu_e}n_B}$
		$\approx 3.3 \times 10^3(\mathrm{sec}^{-1})\rho^{-1/3}_{12}T^7_{11}\frac{F_2(\eta_{\nu_e})}{F_3(\eta_{\nu_e})} < 1 - f_e(\varepsilon) >_{nn}< 1 - f_{\nu_e}(\varepsilon) >_{nn}$
4	$\bar{\nu}_e + p \rightleftharpoons e^+ + n$	$\dot{Y}_{e^+}(\bar{\nu}_ep) \approx 9.0 \times 10^2(\mathrm{sec}^{-1})T_{11}[Y_{pn}F^+_4(\eta_{\bar{\nu}_e}, \eta_{e^+}, -q) - Y_{np}F^-_4(\eta_{\bar{\nu}_e}, \eta_{e^+}, -q)]$
5	$N + N \rightarrow N + N + \nu_i + \bar{\nu}_i$	$\dot{Y}_{\nu_i}(NN) \approx \frac{q_{\nu\bar{\nu}}(nn)}{2\bar{\varepsilon}_{\nu_i}n_B} \approx 1.3(\mathrm{sec}^{-1})X^2_N\rho_{12}T^5_{11}\frac{F_2(\eta_{\nu_i})}{F_3(\eta_{\nu_i})}\left(\frac{3}{2+0.862T_{11}}\right)^{1/2}$
6	$e + e^+ \rightleftharpoons \nu_i + \bar{\nu}_i$	$\dot{Y}_{\nu_e}(ee^+) \approx 36.3(\mathrm{sec}^{-1})T^8_{11}f_{3,\nu_e}(\eta)$
		$\dot{Y}_{\nu_x}(ee^+) \approx 31.2(\mathrm{sec}^{-1})T^8_{11}f_{3,\nu_x}(\eta)$
7	$\gamma \rightarrow \nu_i + \bar{\nu}_i$	$\dot{Y}_{\nu_e}(\gamma) \approx 1.4 \times 10^2(\mathrm{sec}^{-1})F_\gamma(\eta)\rho^{-1}_{11}T^8_{11}$
		$\dot{Y}_{\nu_x}(\gamma) \approx 1.0(\mathrm{sec}^{-1})F_\gamma(\eta)\rho^{-1}_{11}T^8_{11}$

[a]

[a] The parameter b is $b = 4\pi\left(\frac{m_ec}{h}\right)^3$. The complex integrals, $F^{q'+}_4(\eta_{\nu_e}, \eta_e)$ and $F^{q'}_4(\eta_{\nu_e}, \eta_e)$, are shown in Table A5. $f_{3,\nu_i}(\eta)$ and $F_{Q\gamma}(\eta_{\nu_e})$ are $f_{3,\nu_i}(\eta) = (F_3(0))^{-2}\Big\{F_3(\eta_e)F_3(\eta_{e^+}) < 1 - f_{\nu_i}(\varepsilon) >_{ee}< 1 - f_{\bar{\nu}_i}(\varepsilon) >_{ee} - F_3(\eta_{\nu_i})F_3(\eta_{\bar{\nu}_i}) < 1 - f_e(\varepsilon) >_{\nu_i\bar{\nu}_i}< 1 - f_{e^+}(\varepsilon) >_{\nu_i\bar{\nu}_i}\Big\}$, and $F_{Q\gamma}(\eta_{\nu_e}) = \gamma^6e^{-\gamma}\frac{1}{2}((1 + (\gamma + 1)^2) < 1 - f_{\nu_e}(\varepsilon) >_\gamma< 1 - f_{\bar{\nu}_e}(\varepsilon) >_\gamma$. The mean blocking factors $< 1 - f_{\bar{\nu}_e}(\varepsilon) >_\gamma$, ... are described in Table 5. X_N is the mass fraction of neucleons.

uated with the average energy of electrons and positrons produced by e^-e^+-pair creation(Ruffert, Janka, & Schafer 1996):

$$< 1 - f(\eta_{e^+}) >\cong \Big\{1 + \exp\left[-(\bar{\varepsilon}^+ - \eta_{e^+})\right]\Big\}^{-1}. \qquad \text{(C2)}$$

The average energies, $\bar{\varepsilon}^+$ and $\bar{\varepsilon}^-$, are approximately given by

$$\bar{\varepsilon}^+ = \bar{\varepsilon}^- = \frac{\varepsilon_{e^+}}{n_{e^+}} = \frac{7\pi^4}{180\zeta(3)}kT, \qquad \text{(C3)}$$

where ε_{e^+} and n_{e^+} are the energy and number densities of positrons. When the fraction of positrons becomes large, $Y_{e^+} \geqslant 0.01$, the changing rate of positron number, $\dot{n}_{e^+}$, due to the reactions, $e^+ + n \rightleftharpoons \bar{\nu}_e + p$, $e + e^+ \rightleftharpoons \nu_i + \bar{\nu}_i$, cannot be negligible. We calculate the changing rate of the positrons along the flow by using the following equation:

$$\dot{Y}_{e^+} = n^{-1}_b v^r\nabla_r n_{e^+} = n^{-1}_b(\dot{n}_{e^+} + v^r\nabla_r n_{e^+th}), \qquad \text{(C4)}$$

Table A5. Integrals and Blocking Factors

No.	Integrals and Blocking Factors	
1	$F_k^{+}(\eta_\nu,\eta_e,q)=\int_0^\infty \frac{x^{k-2}\Theta(x+q-m)(x+q)^2}{1+\exp{(x-\eta_\nu)}}(1-f_e(q+x))dx=\int_0^\infty \frac{x^{k-2}\Theta(x+q-m)(x+q)^2dx}{(1+\exp{(x-\eta_\nu)})(1+\exp{(\eta_e-q-x)})}$	
2	$F_k^{-}(\eta_\nu,\eta_e,q)=\int_0^\infty \frac{x^{k-2}\Theta(x+q-m)(x+q)^2}{(1+\exp{(x+q-\eta_e)})}(1-f_\nu(x))dx=\int_0^\infty \frac{x^{k-2}\Theta(x+q-m)(x+q)^2dx}{(1+\exp{(x+q-\eta_e)})(1+\exp{(\eta_\nu-x)})}$	
3	$F_k^{q'-}(\eta_\nu,\eta_e)=\int_0^\infty \frac{(x+q')^2x^{k-2}}{\exp{(x+q'-\eta_e)}+1}(1-f_\nu(x))dx=\int_0^\infty \frac{(x+q')^2x^{k-2}dx}{(\exp{(x+q'-\eta_e)}+1)(\exp{(\eta_\nu-x)}+1)}$	
4	$F_k^{q'+}(\eta_\nu,\eta_e)=\int_0^\infty \frac{x^{k-2}(x+q')^2}{1+\exp{(x-\eta_\nu)}}(1-f_e(q'+x))dx=\int_0^\infty \frac{x^{k-2}(x+q')^2dx}{(1+\exp{(x-\eta_\nu)})(1+\exp{(\eta_e-q'-x)})}$	
5	$<1-f_e(\varepsilon)>_{nn}\approx\left\{1+\exp{[\eta_\nu-\frac{F_5(\eta_n}{F_4(\eta_n)}]}\right\}^{-1}$	a
6	$<1-f_\nu(\varepsilon)>_{nn}\approx\left\{1+\exp{[\eta_\nu-\frac{F_5(\eta_n}{F_4(\eta_n)}]}\right\}^{-1}$	
7	$<1-f_{\nu_i}(\varepsilon)>_{ee}\approx\left\{1+\exp\left[\eta_{\nu_i}-\frac{1}{2}\left(\frac{F_5(\eta_e)}{F_4(\eta_e)}+\frac{F_5(\eta_{e^+})}{F_4(\eta_{e^+})}\right)\right]\right\}^{-1}$	
8	$<1-f_e(\varepsilon+q')>\approx\left\{1+\exp\left[\eta_e-\frac{F_5(\eta_{\nu_e})}{F_4(\eta_{\nu_e})}-q'\right]\right\}^{-1}$	
9	$<1-f_{\nu_i}(\varepsilon)>_\gamma\approx\left(1+\exp\left[\eta_{\nu_i}-(1+\frac{1}{2}\frac{\gamma^2}{1+\gamma})\right]\right)^{-1}$	

[a] The quantity $\Theta(x)$ is the unit step function, $\Theta(x)=0$ if $x<0$, and $\Theta(x)=1$ if $x\geqslant 0$.

where $\dot{n}_{e^+}$ is the net production rate of positrons, $\dot{n}_{e^+}=-\dot{n}_{\bar{\beta}}-\dot{n}_{ee}$.

APPENDIX D: DYNAMICAL STRUCTURE OF THE DISK

Dynamically equilibrium structure of the disk is given by the Euler equation. The equation of motion of the fluid, $h_i^kT^j_{k;j}=0$, for the steady, axially symmetric and rotating ideal fluid can be expressed in the total differential form:

$$\frac{dp}{\rho+\epsilon+P}=\gamma^2(-d\nu+v_{(\varphi)}^2d\psi-v_{(\varphi)}v_\omega d\ln\omega)\equiv dU. \qquad \text{(D1)}$$

The equipressure surfaces are given by the equation $U=$constant. The quantity $U=U(p)$ is equal in the Newtonian limit to the total potential (gravitational plus centrifugal ones) expressed in the units of c^2 (Abramowicz, Jaroszyński Sikora 1978). We solve the disk structure in terms of cylindrical coordinates ϖ, z, and φ instead of radial coordinates which are combined through the relations,

$$r\equiv\sqrt{\varpi^2+z^2}, \quad \theta\equiv\cos^{-1}{(z/r)}. \qquad \text{(D2)}$$

If no pressure force exerts in the ϖ direction, the equation (D1) determines the velocity of the geodesic circular orbit, $v_{(\varphi)}$. Let's introduce the new variables, $\tilde{a},\tilde{m},s,c$ defined by $\tilde{a}\equiv a/r$, $\tilde{m}\equiv M/r$, $s\equiv\sin\theta$, $c\equiv\cos\theta$. The following functions are defined by:

$$\begin{aligned}
\Sigma' &= 2rs(1-\tilde{a}^2c^2), \quad \Delta'=2rs(1-\tilde{m})\\
A' &= 2r^3s\Big\{2+\tilde{a}^2(1+\tilde{m}(1+c^2)-\tilde{a}^2c^2)\Big\},\\
A_v &= 2\psi_{,\varpi}=\frac{A'}{A}-\frac{\Sigma'}{\Sigma}+\frac{2c^2}{rs},\\
B_v &= -v_\omega\frac{\partial\ln\omega}{\partial\varpi}=\frac{s}{r}-\frac{A'}{A},\\
C_v &= 2\nu_{,\varpi}=\frac{\Sigma'}{\Sigma}+\frac{\Delta'}{\Delta}-\frac{A'}{A}.
\end{aligned}$$

The circular velocity is then given by

$$v_{(\varphi)}=\frac{-B_v\pm\sqrt{B_v^2+A_vC_v}}{A_v}. \qquad \text{(D3)}$$

This velocity at the equatorial plane is expresses as

$$v_{(\varphi)}=\frac{\Theta_1(r)}{r^{1/2}}, \quad \Theta_1(r)\equiv\frac{1-2aM^{1/2}r^{-3/2}+a^2r^{-2}}{(1-2Mr^{-1}+a^2r^{-2})^{1/2}(1+aMr^{3/2})}. \qquad \text{(D4)}$$

The vertical force is described by the gradient of the equipotential, ∇_zU. The first order of the expansion of $\partial U/\partial z$ in $z/r(\ll 1)$ gives the approximate expression such as

$$\begin{aligned}
\frac{\partial U}{\partial z} &\approx -\frac{Mz}{r^3}\Phi,\\
\Phi(r) &= \frac{1-\omega/\Omega}{D}\big(\frac{\gamma\Psi}{\Theta}\big)^2\Big\{1+\frac{1+v_{(\varphi)}^2}{v_{(\varphi)}v_\Omega}\big[1+(\frac{a}{r})^2\big]\\
- &\quad (1+\frac{\omega}{\Omega}+\frac{1}{v_{(\varphi)}v_\Omega})\frac{\acute{A}}{\Psi}+\frac{1-M/r}{v_{(\varphi)}v_\Omega D}\Big\},\\
\Theta(r) &= 1+\frac{aM^{1/2}}{r^{3/2}}, \quad D=1-\frac{2M}{r}+\big(\frac{a}{r}\big)^2,\\
\Psi &= 1+\big(\frac{a}{r}\big)^2\big(1+2\frac{M}{r}\big),\\
\acute{A} &= 2+(4-3\frac{M}{r})\big(\frac{a}{r}\big)^2+\big(\frac{a}{r}\big)^4,\\
v_\Omega &= \Omega e^{\psi-\nu}=v_{(\varphi)}+\omega e^{\psi-\nu}
\end{aligned} \qquad \text{(D5)}$$